journal

J. Am. Ceram. Soc., **81** [8] 1977–94 (1998)

Indentation of Ceramics with Spheres: A Century after Hertz

Brian R. Lawn*

Materials Science and Engineering Laboratory, National Institute of Standards and Technology, Gaithersburg, Maryland 20899

In this article we review the nature and mechanics of damage induced in ceramics by spherical indenters, from the classical studies of Hertz over a century ago to the present day. Basic descriptions of continuum elastic and elastic–plastic contact stress fields are first given. Two distinct modes of damage are then identified: Hertzian cone cracks, in relatively hard, homogeneous materials, such as glasses, single crystals, fine-grain ceramics (tensile, ''brittle'' mode); and diffuse subsurface damage zones, in relatively tough ceramics with heterogeneous microstructures (shear, ''quasi-plastic'' mode). Ceramographic evidence is presented for the two damage types in a broad range of materials, illustrating how an effective brittle–ductile transition can be engineered by coarsening and weakening the grain structure. Continuum analyses for cone fracture and quasi plasticity, using Griffith–Irwin fracture mechanics and yield theory, respectively, are surveyed. Recent micromechanical models of the quasi-plastic mode are also considered, in terms of grain-localized ''shear faults'' with extensile ''wing cracks.'' The effect of contact-induced damage on the ensuing strength properties of both brittle and quasi-plastic ceramics is examined. Whereas cone cracking causes abrupt losses in strength, the effect of quasi-plastic damage is more gradual—so that more heterogeneous ceramics are more damage tolerant. On the other hand, quasi-plastic ceramics are subject to accelerated strength losses in extreme cyclic conditions (''contact fatigue''), because of coalescence of attendant microcracks, with implications concerning wear resistance and machinability. Extension of Hertzian contact testing to novel layer structures with hard, brittle outer layers and soft, tough underlayers, designed to impart high toughness while preserving wear resistance, is described.

D. B. Marshall—contributing editor

Manuscript No. 190382. Received February 13, 1998; approved June 22, 1998.
*Member, American Ceramic Society.

I. Introduction

SINCE Hertz first investigated the beautiful cone-shaped fractures produced in contacts between glass lenses in the 1880s (see *Hertz's Collected Papers*[1]), indentation mechanics has become extensively used in the analysis and characterization of fracture and deformation properties of brittle ceramics,[2,3] as well as of metals and other materials.[4] Indentation damage bears profoundly on a wide range of other mechanical properties, such as strength, toughness, and wear. Such damage is now recognized as a key limiting factor in the lifetime of ceramics in many engineering applications,[2,3,5] especially bearings[6] and engine components,[7] in both monoliths and coatings. Indentation damage applications extend to areas as diverse as dental restorations[8] and the anthropological study of ancient tools.[9] Accordingly, it is timely in this centennial feature article to review the nature and mechanics of contact damage, with due attention to both its rich historical basis in brittle fracture and its topical applications in the latest generation of tough ceramics.

Traditionally, Hertzian cone cracks have been most widely studied in flat silicate glass plate, using spheres of hard steel or tungsten carbide. Extensions to other brittle solids, single crystals (especially those with the diamond structure) and some hard, fine-grain polycrystalline ceramics became more prevalent in the period 1950–1970.[3] The Hertzian fracture begins as a surface ring crack outside the elastic contact and then, at a critical load, propagates downward and flares outward within a modest tensile field into a stable, truncated cone configuration. Much of the early work centered on the mechanics of cone crack initiation, especially the empirically observed linear relation between critical load and sphere size, so-called Auerbach's law, dating from 1891.[10] Auerbach's law posed a paradox, in that it apparently violated the notion that cone cracks should initiate when the maximum tensile stress in the indented body exceeds the bulk strength of the material. Griffith–Irwin fracture mechanics analysis was first introduced in the late 1960s to account for this paradox,[11] with many refinements and reinventions during the ensuing three decades.

More recently, sphere-indentation methods have been extended to heterogeneous ceramics with weak internal interfaces, large and elongate grains, and high internal residual

centennial feature

stresses—i.e., tougher ceramics characterized by *R*-curves. The *R*-curve can be due to several toughening mechanisms, but is most commonly associated with energy dissipation by internal friction at sliding grains, platelets or whiskers, or other microstructural elements that ''bridge'' the crack wake.[12–14] Such ceramics ordinarily appear completely brittle in traditional strength tests. However, the very same microstructural features that enhance long-crack toughness tend also to degrade short-crack toughness, compromising such important properties as wear resistance.[15] Hertzian fracture tends to be suppressed in these materials—instead, a ''quasi-plastic'' deformation zone develops in the strong shear–compression region below the contact. Macroscopically, this deformation region resembles the plastic zones that occur in metals.[4] Microscopically, however, the damage is altogether different, consisting of an array of ''closed'' mode II cracks with internal sliding friction (''shear faults'') at the weak planes within the microstructure.[16] At high loads, secondary ''extensile'' microcracks initiate at the ends of the constrained faults. Much precedent for this type of distributed damage exists in the literature on grossly heterogeneous brittle rocks in confined compression fields.[17,18] It is implicit that one can control the degree of quasi plasticity relative to the brittle mode by suitably tailoring the ceramic microstructure.[16]

Experimental simplicity and amenability to materials evaluation are features of general indentation testing. Sometimes indentation is the only practical means of obtaining fundamental information on critical lifetime-limiting damage modes in some ceramics, particularly the quasi-plastic mode. However, we will not attempt to cover the entire field of indentation testing here, omitting in particular parallel developments in the 1970s using Vickers and Knoop indenters (''sharp'' indenters). These parallel developments have been reviewed elsewhere.[2,3,5] We simply point out here one major advantage of ''blunt,'' spherical indenters—they enable one to follow the entire evolution of damage modes, as a progressive transition from initial elasticity to full plasticity.[19]

The layout in this article is as follows. We begin with a consideration of the stress fields beneath a spherical indenter, in both elastic and elastic–plastic contact. Then we present micrographic evidence for the two modes of indentation damage, single cone cracking (''brittle mode'') and distributed microdamage (''quasi-plastic mode''), in a broad range of glassy and polycrystalline ceramics. Specific attention is focused on the controlling role of microstructure in the competition between these two modes. Damage models for the two modes, at both the macroscopic and microscopic levels, are described. The practical issue of strength degradation from damage accumulation, in particular relation to damage tolerance, is then examined. Finally, the scope of Hertzian contact testing is illustrated by examining the most recent work on contact fatigue and damage in layer structures.

II. Contact Stress Fields

Consider the frictionless contact of a sphere, radius r, at normal load P, on a flat continuum specimen, Fig. 1. The field is initially elastic. Beyond a critical load, either a Hertzian cone crack (''brittle solid'') or a subsurface deformation zone (''plastic solid'') initiates. Here we outline the basic features of the stress fields associated with elastic and elastic–plastic contacts.

(1) Elastic Fields

The basic Hertzian elasticity solutions for a sphere of radius r at normal load P are well documented.[1,2,20,21] The contact radius a is given by

$$a^3 = 4kPr/3E \tag{1}$$

where E is Young's modulus and $k = (9/16)[(1 - \nu^2) + (1 - \nu'^2)E/E']$ is a dimensionless coefficient, with ν Poisson's ratio and the prime notation denoting the indenter material.[21] The

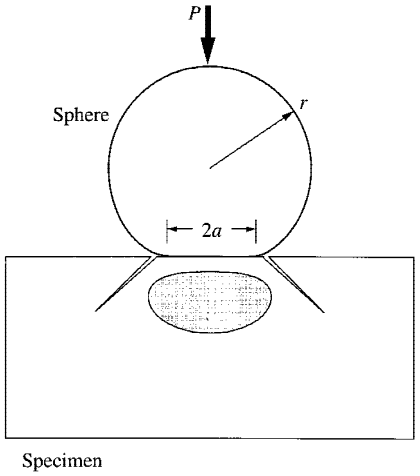

Fig. 1. Hertzian contact of sphere on flat ceramic specimen. Beyond elastic limit, contact initiates cone fracture (''brittle mode'') or subsurface deformation zone (''quasi-plastic mode'').

contact radius defines the spatial scale of the contact field. The mean contact pressure

$$p_0 = P/\pi a^2 \tag{2}$$

defines the intensity of the contact field. The maximum tensile stress in the specimen occurs at the contact circle:

$$\sigma_m = \frac{1}{2}(1 - 2\nu)p_0 \tag{3}$$

The maximum shear stress is located along the contact axis at a depth $\approx 0.5a$ below the surface:

$$\tau_m \approx 0.48p_0 \tag{4}$$

The mean contact pressure in Eq. (2) can be written in other useful forms by combining with Eq. (1). One such form expresses p_0 in terms of a and r:

$$p_0 = (3E/4\pi k)a/r \tag{5}$$

Equation (5) prescribes a linear relation between p_0, ''indentation stress,'' and a/r, ''indentation strain,'' leading to a procedure for obtaining basic stress–strain information.[4,22] Another useful form is given in terms of P and r:

$$p_0 = (3E/4k)^{2/3}(P/\pi r^2)^{1/3} \tag{6}$$

Principal normal and shear stresses are calculable from analytical solutions of the contact boundary conditions (Panel A). It is conventional to define $\sigma_1 \geq \sigma_2 \geq \sigma_3$ nearly everywhere within the Hertzian field, so that σ_1 is the most tensile principal stress and $\tau_{13} = \frac{1}{2}(\sigma_1 - \sigma_3)$ is the maximum principal shear stress. Figure 2 shows contours of σ_1, σ_3, and τ_{13} (σ_2 is a ''hoop'' stress). The σ_1 tensile stresses (shaded) in Fig. 2(a) concentrate in a shallow surface region, with maximum value σ_m at the contact circle (Eq. (3)). Included in Fig. 2(a) are σ_3 stress trajectories (dashed lines) from the specimen surface, defining paths always normal to σ_1 within the plane of the diagram. The rapid decrease of σ_1 along these trajectories is a characteristic feature of contact problems. Note that the σ_3 stresses in Fig. 2(b) are everywhere compressive. The principal shear stresses τ_{13} in Fig. 2(c) are constrained beneath the contact, with widely spaced contours and maximum value τ_m along the contact axis (Eq. (4)).

(2) Elastic–Plastic Fields

Above some yield point relatively soft materials, such as metals, undergo plastic flow beneath the contact. In relation to the uniaxial compression yield stress Y, the flow initiates at $\tau_m = \frac{1}{2}Y = 0.47p_Y$, corresponding to $p_Y \approx 1.1Y$.[4,21] At in-

Panel A. Hertzian Stress Fields

The stresses within the Hertzian elastic contact field are given by the following expressions, in cylindrical coordinates R,θ,z (with z along the axis of symmetry):[21,23]

$$\sigma_R/p_0 = \frac{1}{2}(1-2\nu)(a/R)^2[1-(z/u^{1/2})^3] + \frac{3}{2}(z/u^{1/2})\,[(1-\nu)u/(a^2+u) + (1+\nu)(u^{1/2}/a)\arctan(a/u^{1/2}) - 2]$$

$$\sigma_\theta/p_0 = \frac{1}{2}(1-2\nu)(a/R)^2[1-(z/u^{1/2})^3] + \frac{3}{2}(z/u^{1/2})^3[a^2u/(u^2+a^2z^2)] + \frac{3}{2}(z/u^{1/2})[(1-\nu)u/(a^2+u) + (1+\nu)(u^{1/2}/a)\arctan(a/u^{1/2}) + 2\nu]$$

$$\sigma_z/p_0 = \frac{3}{2}(z/u^{1/2})^3[a^2u/(u^2+a^2z^2)]$$

$$\tau_{Rz} = \frac{3}{2}[Rz^2/(u^2+a^2z^2)][a^2u^{1/2}/(a^2+u)]$$

where

$$u = \frac{1}{2}\{(R^2+z^2-a^2) + [(R^2+z^2-a^2)^2 + 4\,a^2z^2]^{1/2}\}$$

The principal normal stresses, defined such that $\sigma_1 \geq \sigma_2 \geq \sigma_3$ nearly everywhere,[11] are

$$\sigma_1 = \frac{1}{2}(\sigma_R+\sigma_z) + \left\{\left[\frac{1}{2}(\sigma_R+\sigma_z)\right]^2 + \tau_{Rz}^2\right\}$$

$$\sigma_2 = \sigma_\theta$$

$$\sigma_3 = \frac{1}{2}(\sigma_R+\sigma_z) - \left\{\left[\frac{1}{2}(\sigma_R+\sigma_z)\right]^2 + \tau_{Rz}^2\right\}$$

where σ_2 is a hoop stress. The maximum principal shear stress is

$$\tau_{13} = \frac{1}{2}(\sigma_1-\sigma_3)$$

The angle α between the σ_2–σ_3 stress trajectory surface (closely approximating the cone crack path) and the specimen free surface is given by

$$\tan 2\alpha = -2\tau_{Rz}/(\sigma_R-\sigma_z)$$

Analogous relations exist for a cylindrical flat punch end-loaded onto the specimen surface[21] and for a sliding spherical indenter.[24,25]

creasing load the plastic zone expands, but remains constrained within the elastic surrounds, enabling p_0 to increase steadily beyond p_Y, until a state of full plasticity is ultimately attained. In this region the Hertzian field is significantly modified. General analytical solutions for the transitional elastic–plastic field are not available. An ''expanding-cavity'' model embodying a spherically symmetrical half-spherical fully plastic zone encased in an elastic surround has been used with some success in soft metals with negligible strain-hardening in the region of fully plasticity.[21,26] However, the expanding-cavity model breaks down in harder materials with pronounced strain-hardening characteristics, which includes most ceramics.[27,28]

As foreshadowed in the previous subsection, the transition from elastic to plastic contacts can be conveniently demonstrated on indentation stress–strain curves, $p_0(a/r)$ (independent of sphere size r—geometrical similarity[4]). The development of plasticity becomes evident as an ever-increasing deviation from linearity in Eq. (5). Some heterogeneous ceramics, notwithstanding their incapacity to attain full plasticity, are nevertheless sufficiently deformable in sphere indentation to show significant nonlinearities on indentation stress–strain curves[16,22,29] (although generally much less pronounced than in metals). An extreme case is shown in Fig. 3, for a relatively soft micaceous glass-ceramic (Macor, Corning Inc., Corning, NY), noteworthy for its machinability.[30–32] The plot includes data for the material in its brittle base glass state. Above $p_0 = p_Y$ (indicated in Fig. 3) the quasi-plastic glass-ceramic shows distinctive yield characteristics (corresponding to the formation of well-defined residual impressions—see Section IV(1)). Clearly, the microstructural state of the material is crucial to the damage response.

In the absence of an analytical model for describing the indentation stress–strain response in ceramics, one usually resorts to numerical modeling of the contact process, e.g., finite-element modeling (FEM).[27,28] A constitutive yield condition is incorporated into the FEM algorithm, in conjunction with a bilinear stress–strain curve $\sigma(\varepsilon)$ in ideal uniaxial compression for each material (including the indenter):

$$\sigma = E\varepsilon \qquad (\sigma \leq Y) \tag{7a}$$

$$\sigma = Y + \alpha(\varepsilon E - Y) \qquad (\sigma \geq Y) \tag{7b}$$

where E is Young's modulus, Y is the uniaxial yield stress, and α is a dimensionless strain-hardening coefficient in the range $0 \leq \alpha \leq 1$ (with $\alpha = 0$ fully plastic and $\alpha = 1$ fully elastic). (Physical justification for Eq. (7) is given in Section IV(2).) The solid curves through the data in Fig. 3 are FEM-generated $p_0(a/r)$ functions, with independent determinations of E and Y and adjustments of α to give best fits.[28]

III. Hertzian Cone Fracture in Brittle Solids

(1) Historical Survey

As indicated, most early experiments on cone fracture were conducted on glass, notably soda–lime glass, in normal static loading. The transparency of this model brittle solid made it especially easy to follow the crack evolution. The 1950s saw the first serious attempts to understand the underlying mechanics of cone fracture in glass, highlighted by the systematic studies of Tillett[33] and Roesler.[34,35] Around the same time, papers on single crystals, notably on diamond,[36–39] germanium,[40] and silicon[41] began to appear, attesting to the generality of the phenomenon. The main distinguishing features in the single crystals were attendant cleavage tendencies in the surface crack patterns, reflecting crystallographic symmetries.

A photograph of a Hertzian cone crack in glass (in this instance, formed with an axisymmetric flat punch) is shown in Fig. 4(a).[34] The fully developed cone crack is the archetypical stable fracture system.[3,42] The crack base continues to grow steadily with subsequent increasing load. Roesler, using energy balance concepts in conjunction with Tillett's data, established the now well-known relation $P/R^{3/2} = constant$ between applied load P and cone base radius R. In the case of a spherical indenter, the expanding contact circle ultimately engulfs the surface ring, resulting in the generation of secondary ring cracks (a complication avoided with flat-punch indenters). Af-

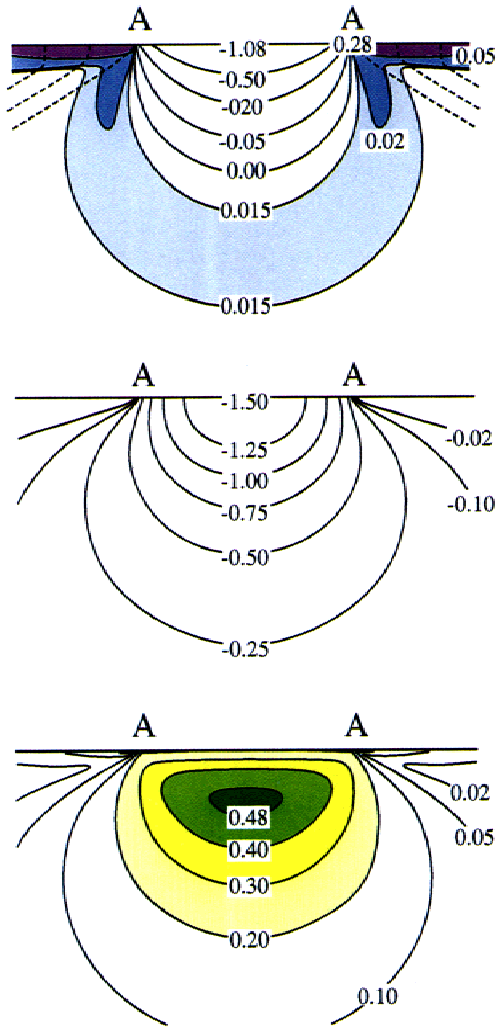

Fig. 2. Hertzian stress field: (a) principal normal stress σ_1, (b) principal normal stress σ_3, and (c) principal shear stress $\tau_{13} = \frac{1}{2}(\sigma_1 - \sigma_3)$. Dashed curves in (a) are σ_3 stress trajectories. Stresses in units of p_0. AA denotes contact diameter $2a$. Plotted for $\nu = 0.22$.

ter unloading, the fracture usually remains visible because of imperfect closure at the crack interface.[39,43]

The mechanics of cone crack *initiation* goes back to 1891, when Auerbach established his famous empirical law between critical load and sphere radius, $P_C \propto r$.[10] This relation and its limits were illustrated most compellingly by Tillett's data on glass,[33] reproduced in Fig. 5 as a plot of P_C/r vs r. Two regions of behavior are evident: the Auerbach region, $P_C/r = constant$, at small r; and a second region, asymptotic to $P_C/r^2 = constant$, at large r. Roesler subsequently reviewed the existing literature data on glass and demonstrated the commonality of Auerbach's law under a wide range of contact conditions, including impact.[35] From such studies arose one of the most celebrated paradoxes in brittle fracture theory: if it is assumed that cone cracking initiates when the maximum tensile stress exceeds the strength of the bulk solid, $\sigma_C = \sigma_m = \sigma_F$, Eqs. (3) and (6) predict $P_C \propto r^2$, independent of r. As Fig. 5 shows, this quadratic relation is approached only in the limit of infinite r. The stresses σ_C calculated from Eqs. (3) and (6) using measured P_C values are invariably higher than the measured bulk strengths σ_F on the same material, the more so at smaller r, implying breakdown of the critical stress concept; specifically, $P_C \propto r$ corresponds to $\sigma_m \propto r^{-1/3}$. At sufficiently small r, σ_C may become high enough that some form of plasticity generates before fracture, in even the most brittle materials, indicating a ''brittle–ductile'' transition with increasing indenter

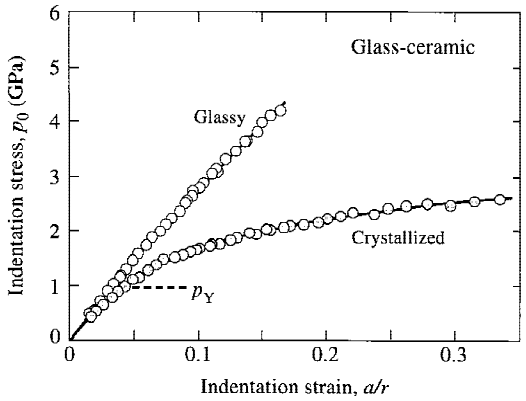

Fig. 3. Indentation stress–strain curve for glass-ceramic, in base glass and crystallized forms. Data taken with tungsten carbide spheres in the radius range $r = 0.79$ mm to 12.7 mm (not distinguished in plot). Curves through data are FEM fits using Eq. (7), with $\alpha = 1$ for the glassy state and $\alpha = 0.10$ for the crystallized state (E and Y independently determined). Initial yield pressure p_Y indicated for glass-ceramic. Data reproduced from Refs. 16 and 32.

''sharpness.''[29,44–47] At the same time, σ_C generally remains well below the limiting cohesive strength of the solid over most practical ranges of r, indicating that the cone cracks must initiate from pre-present flaws.

This last point raises the issue of flaw statistics.[48,49] At one time it was proposed that Auerbach's law might be explained if the flaw distributions were sufficiently sparse. Assuming that the critical stress criterion remains valid, it was argued that smaller contacts have a lower probability of locating larger flaws within a given size population, accounting for an apparent increase in critical stress with decreasing r. This school pointed to the wide scatter in P_C data on smooth, carefully handled glass surfaces. However, later experiments on glass surfaces containing controlled flaws introduced by a wide range of abrasive grit sizes demonstrated an insensitivity of P_C to flaw size in the Auerbach region.[50]

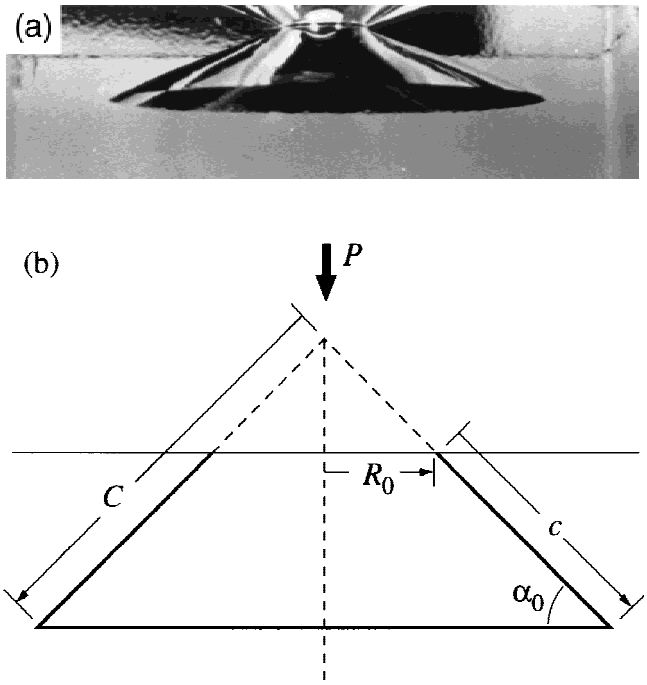

Fig. 4. Hertzian cone fracture: (a) photograph of crack in soda–lime glass, produced by indentation with cylindrical punch at $P = 40$ kN (block edge 50 mm), from Ref. 34; and (b) schematic showing critical geometrical parameters.

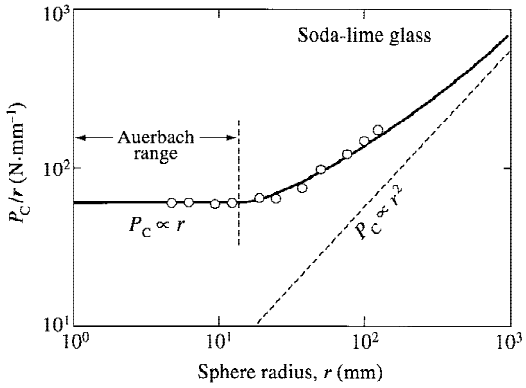

Fig. 5. Plot of P_C/r vs r for polished soda–lime glass, using steel spheres. Inclined dashed line is prediction for flaw in uniform field σ_m. Plot reproduced from Ref. 50, using Tillet's data.[33]

An important factor in the evolution of cone cracking is the test environment, particularly water. Early experimentalists noted that newly formed cone cracks in glass extend steadily at constant load, at first rapidly and then more slowly.[34,51] This growth was later demonstrated to be commensurate with conventional crack velocity laws.[52,53] The role of moisture is even stronger in the crack initiation. Figure 6 shows some data for soda–lime glass indented with steel spheres in different environments, plotted as critical load P_C vs contact time t_C (time to fracture at constant crosshead speed).[54] In any given environment, P_C decreases steadily with increasing t_C. At any given t_C, P_C decreases with increasing water content and with increasing temperature, highlighting the kinetic effect. Section-and-etch studies on cracks grown slowly in moist environments confirmed that the cone begins its life as a slowly penetrating embryonic surface ring prior to its abrupt full development.[55]

Later, experiments were extended to fine-grain polycrystalline and other ceramics.[56–63] Such materials are generally opaque, making it necessary to observe the specimen surface *a posteri* or to use acoustic emission to detect the crack initiation.

(2) Introduction of Fracture Mechanics

Introduction of Griffith–Irwin fracture mechanics into the Hertzian fracture problem was made in 1967 by Frank and Lawn,[11] with the express purpose of deriving Auerbach's law from first principles. The basic precepts of the fracture mechanics approach in the context of Hertzian fracture can be summarized as follows. Cone cracks tend to form in highly brittle solids with zero or insignificant *R*-curves, i.e., materials with single-valued toughness, $K_{IC} = T_0$. For such materials, extension of any crack of length c under equilibrium conditions is determined by the simple equality $K(c) = T_0$: if $dK(c)/dc > 0$, the equilibrium is unstable; if $dK(c)/dc < 0$, the equilibrium is stable.[3] When kinetic conditions prevail, extension is determined by a crack velocity relation $v = v(K)$.

Consider cone cracks in their well-developed state, Fig. 4(b). The actual crack length c is related to the dimension C of a ''virtual'' cone with the tip located above the contact surface:

$$C = c + R_0/\cos\alpha_0 \tag{8}$$

where R_0 is the surface ring radius and α_0 is the cone base angle. The stress-intensity factor for this virtual cone crack system is given by[3]

$$K(c) = \chi P/C^{3/2} \tag{9}$$

where χ is a crack geometry coefficient. At $K = T_0$, we have $P \propto C^{3/2}$, i.e., Roesler's relation. Sphere radius r enters Eqs. (8) and (9) only through R_0; therefore, $K(c)$ is insensitive to r in the region $c >> R_0$.

The mechanics of cone crack initiation is more complex. The Frank–Lawn treatment[11] addressed this issue in two key steps:

(i) The cone cracks start from flaws on the specimen top surface at (or just outside) the contact circle where the tensile stresses are concentrated. The embryonic cracks subsequently circumvent the contact circle as a shallow surface ring, then propagate downward and outward, closely (but not exactly) following the σ_3 trajectories (so as to be nearly normal at all points to the σ_1 tensile stresses) in the *prior* stress field (Fig. 2(a)).

(ii) A stress-intensity factor for the downward crack extension can be expressed uniquely in terms of the prior stress function $\sigma_1(s)$, where s is a coordinate along the σ_3 trajectory. The stress-intensity factor has the form

$$K(c/a) = p_0 a^{1/2} I(c/a,\beta,\nu) \tag{10}$$

where $\beta = R_0/a$ is the relative crack location and $I(c/a,\beta,\nu)$ is the dimensionless integral

$$I(c/a,\beta,\nu) = 2(c/\pi a)^{1/2} \int_0^{c/a} [\sigma_1(s/a,\beta,\nu)/p_0]\, d(s/a)/(c^2/a^2 - s^2/a^2)^{1/2} \tag{11}$$

Figure 7 sketches the normalized function $K(c/a)/T_0$ for a sequence of increasing loads ($P' \rightarrow P'' \rightarrow P'''$). The function has two unstable branches (1,3) and two stable (2,4) branches. Suppose the specimen contains surface flaws within the range $c_0 \leq c_f \leq c_*$ and that equilibrium conditions prevail. Then the crack evolves along the configurational path marked by the arrows, growing stably with load along $K/T_0 = 1$ until a critical penetration depth $c = c_*$ is reached, whence the full cone crack pops in and arrests on branch 4. Inserting $I_* = I(c_*/a) = constant$ and using Eqs. (1) and (2) to eliminate p_0 and a in Eq. (10), we obtain the critical condition for cone initiation:

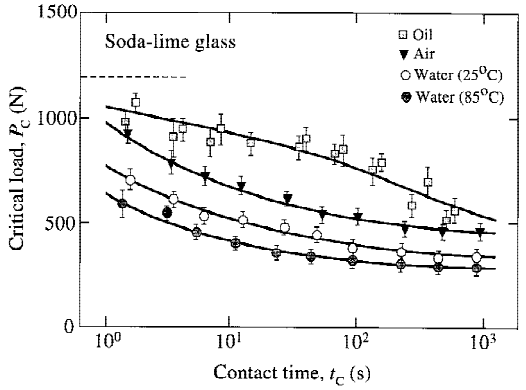

Fig. 6. Critical load for cone initiation as function of time to fracture in surface-abraded soda–lime glass, using steel spheres ($r = 6.35$ mm) at constant crosshead speeds in different environments. Reference horizontal dashed line is ''inert'' value (evaluated from sphere drop tests). Data from Ref. 54.

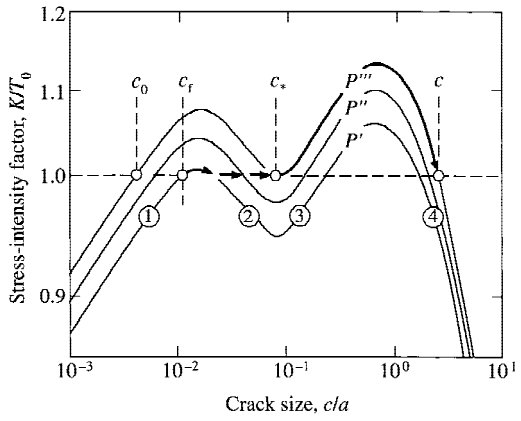

Fig. 7. Normalized $K(c)$ curves for Hertzian fracture ($\beta = 1$ and $\nu = 0.3$). Arrows indicate evolution from surface flaw to full cone crack. Plots from Refs. 2 and 3.

$$P_C/r = AT_0^2/E = constant \quad (12)$$

where $A = 4\pi^2 k/3I_*^2 = constant$. Equation (12) is a formal statement of Auerbach's law.

The requirement that surface flaws must first grow to depth c_* before propagating into the full cone renders P_C independent of c_f in Eq. (12), consistent with the test results on variously abraded glass surfaces mentioned in the previous subsection.[50] For very small flaws in the range $c_f << c_0$, or for very large spheres (large r, large a), the initiation is spontaneous from branch 1 to branch 4—this is the domain of the asymptotic relation $P_C \propto r^2$ in Fig. (5). Interestingly, for very large flaws in the range $c_f >> c_*$ it can become increasingly difficult to initiate cone cracks at all, because of difficulties in accommodating the crack to the curved stress trajectory paths of maximum tension.[50,64,65]

A feature of Eq. (12) is the appearance of toughness T_0 (not apparent, of course, in the original empirical Auerbach's law).[11,34] This feature has been used to evaluate the toughness properties of several brittle glasses and single crystals[2,11,66,67] and fine-grain ceramics[58–63] (although Vickers indenters have proved to be more popular in this regard[68,69]).

Several variants of the above theory have appeared in the three decades since 1967.[53,61,70,71] Most have focused on modifications to the Greens function in Eq. (11), with allowance for several factors: a starting surface crack outside the contact ($\beta > 1$);[70,72] indenter–specimen interface friction (which redistributes the tensile stresses);[73] an ever-widening crack front;[53] and hybrid combination of flaw statistics with fracture mechanics.[71] One conclusion that can be drawn from these variant studies is that the exact form of the calculated $P_C(r)$ function is highly assumption-sensitive, making absolute predictions of toughness difficult. Some analyses question the existence of the ''energy barrier'' at $c = c_*$ in Fig. 7. In this context of analytical subjectivity, an approach by Kocer and Collins[74] using FEM simulations of cone crack evolution is worthy of special mention. In their algorithm, the cone crack is allowed to grow stepwise from a starting surface flaw, and the *actual* (as distinct from the *prior*) field at the crack tip is reevaluated at each step, using energy-release-rate principles to determine the next increment. The Kocer–Collins procedure is noteworthy for its accurate prediction of the observed cone crack angle, and offers the prospect of more-objective evaluations of toughness parameters.

Notwithstanding any persistent uncertainties in the fracture mechanics, the stabilizing role of the decreasing tensile stress function $\sigma_1(s)$ in Eq. (11) in the experimentally documented shift away from $P_C \propto r^2$ toward $P_C \propto r$ and the associated sphere-size dependence of the critical tensile stress σ_C are incontrovertible.

Finally, how restrictive is the presumption of a single-valued toughness in the equilibrium-crack analyses? For microstructurally heterogeneous ceramics with R-curves, $K(c)$ in Eqs. (9) and (10) should strictly be equated to a crack-size-dependent toughness function $K_R(c) = T(c)$ rather than to T_0 (equivalent to replacing the horizontal dashed line at $K/T_0 = 1$ in Fig. 7 by a K_R-curve), with consequent reduction in size of the cone crack. But a more dramatic consequence of microstructural heterogeneity, as shown in the next section, is a fundamental change in the damage mode.

IV. Quasi-Plastic Damage in Tough Ceramics

(1) Nature of Quasi-Plastic Deformation

Investigation of sphere-indentation quasi-plastic damage in tough, heterogeneous ceramics, although foreshadowed in some earlier studies,[22,29,75] began in earnest only in the 1990s.[16,19,32,76–79] We have already alluded to this damage mode in association with nonlinear stress–strain curves (Fig. 3) and to attendant suppression of cone cracking in such ceramics. The question remains: what is the nature of the quasi plasticity?

Contact-induced quasi plasticity is manifest as a residual surface impression above a threshold yield load P_Y. Combining $\tau_m = \frac{1}{2}Y$ with Eqs. (4) and (6) gives

$$P_Y/r^2 = (1.1\pi Y)^3(4k/3E)^2 = constant \quad (13)$$

Measurement of p_Y thereby affords a simple means for determining the yield stress Y.[80] The quadratic relation $P_Y \propto r^2$ implies geometrical similarity in the elastic–plastic field (valid as long as the contact dimension remains very much larger than the microstructure scale[4,81]). Again, comparison of $P_Y \propto r^2$ for yield with $P_C \propto r$ for cracking indicates an increasing tendency to dominant plasticity at ''sharper'' contacts.

But the most informative clues as to the nature of the quasi-plastic mode are obtained from subsurface sections. (Recall from Fig. 2(c) that the location of maximum shear stress is located beneath the contact surface.) One particularly useful technique, an adaptation from earlier workers,[29,82,83] involves *pre*sectioning a specimen into two half-blocks before indentation, using an adhesive to bond the two halves together again, and indenting across the surface trace of the bonded interface—Nomarski illumination of the separated half-blocks then reveals the subsurface damage.[32,76] Half-surface and section views obtained in this way are shown in Fig. 8(a) for the same crystal-

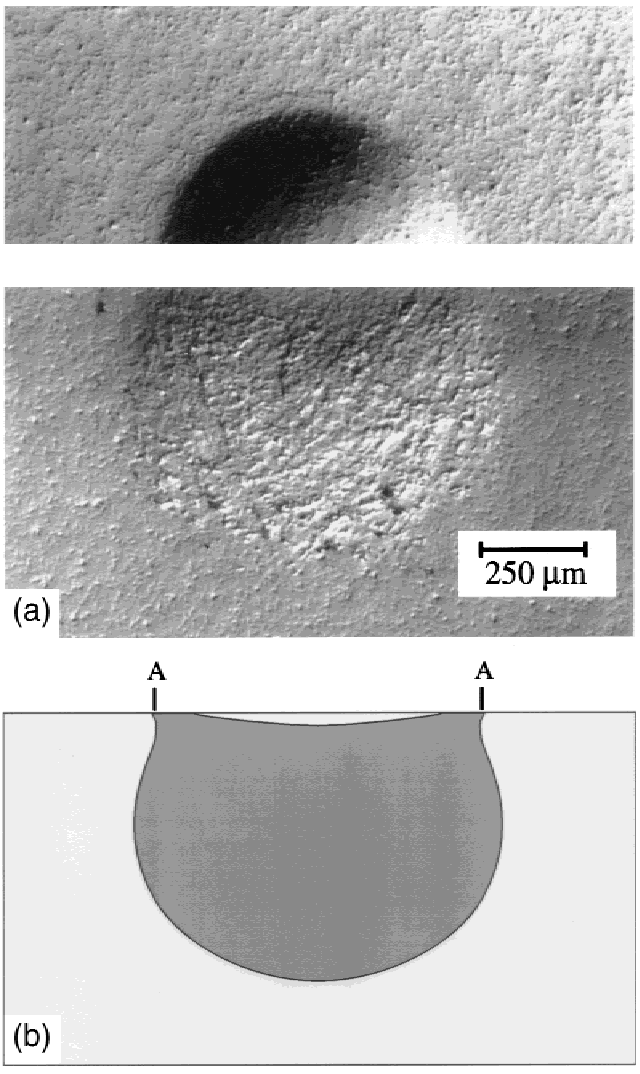

Fig. 8. Hertzian indentation damage in machinable glass-ceramic, from tungsten carbide sphere ($r = 1.98$ mm and $P = 1000$ N): (a) optical micrographs, half-surface and side view of indentation, bonded-interface specimen, surfaces gold coated after indentation, Nomarski interference, from Ref. 32; and (b) computed yield zone, contact diameter AA, using FEM algorithm, from Ref. 28.

lized glass-ceramic used to obtain the stress–strain data in Fig. 3. The subsurface quasi-plastic zone in this ceramic is macroscopically similar to the yield zones beneath hardness impressions in soft metals, except that it is much more highly constrained (''pinched'') beneath the immediate contact. Observations of sequences of indentations at different loads allow one to follow the entire evolution of the quasi-plastic zone, from initial yield to ''full plasticity.''[28,32] Cone cracking is conspicuously absent in Fig. 8(a).

Bonded-interface observations on two other model ceramic systems serve to demonstrate the critical role of microstructure in the competition between fracture and deformation. Figure 9 shows damage patterns in pure, dense alumina over a broad range of grain sizes, 3–48 μm, under common indentation conditions.[19,76] A progressive ''brittle–ductile'' transition with increasing grain size, from well-defined cone cracking to diffuse subsurface damage, is apparent. Surface ring cracks form in all cases, but are increasingly inhibited in their downward growth in the coarser aluminas, ultimately to one grain depth or less. The quasi-plastic zones again remain severely constrained below the contact. The intensity of damage in such zones can be strongly enhanced in the alumina microstructure by including platelet phases with weak interphase boundaries[84,85] or pores.[86] Figure 10 is an analogous sequence of patterns in silicon nitride for microstructures with increasing grain size, aspect ratio, and β:α phase ratio, designated fine (F), medium (M), and coarse (C).[79,81] Once more, a progressive transition from well-defined cone crack to distributed subsurface damage is observed. In this material the response is highly sensitive to processing conditions, starting powder, etc.[87] It is interesting that the grades of silicon nitride used in practical bearing structures lie closest to the intermediate microstructure in Fig. 10,[81] suggesting a compromise between the extremes of dominant cracking and dominant quasi plasticity.

It is at the microstructural level that the underlying character of the quasi-plastic deformation is determined. Figure 11 is a magnified view of the damage in the glass-ceramic of Fig. 8(a), from a central section region.[32] Distributed shear-fault microfailures occur at weak interfaces between mica platelets and surrounding glass phase. (These weak interfaces enhance both machinability[30,31] and long-crack toughness.[88]) Other platelet structures, e.g., alumina with additive calcium hexaluminate phases[84,89] and silicon carbide with yttrium aluminum garnet (YAG) second phase,[77,90] exhibit similar shear-fault arrays. In monolithic structures, e.g., alumina (Fig. 9)[19,76] and silicon nitride,[79] the shear faults take the form of transgranular twinning or block slip. In zirconia, the shear-fault damage is augmented by phase transformations.[78,91] A general feature of the shear faults is their discreteness, localized by the grain structure. The constrained shear faults may in turn initiate secondary microcracks at their ends, especially where the faults intersect weak grain or interphase boundaries.[19,76]

Attempts at quantitative evaluation of the damage intensity have been made. Damage intensity is usually characterized

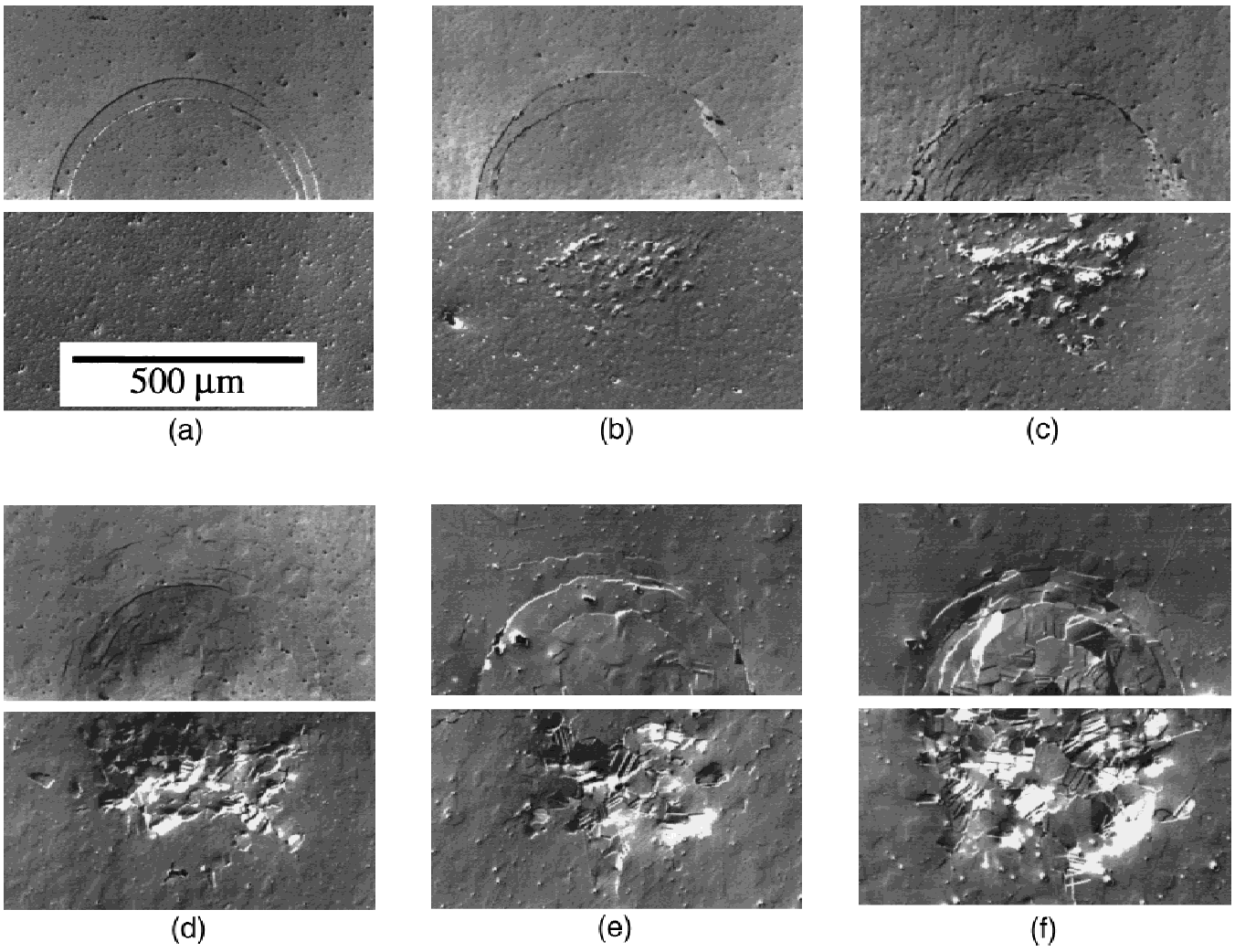

Fig. 9. Hertzian indentation damage in pure, dense alumina from tungsten carbide sphere ($r = 3.18$ mm and $P = 2000$ N), grain sizes (a) 3, (b) 9, (c) 15, (d) 21, (e) 35, and (f) 48 μm. Half-surface (upper) and section (lower) views, bonded-interface specimens. Optical micrographs, surfaces gold coated after indentation, Nomarski interference. Reproduced from Ref. 76.

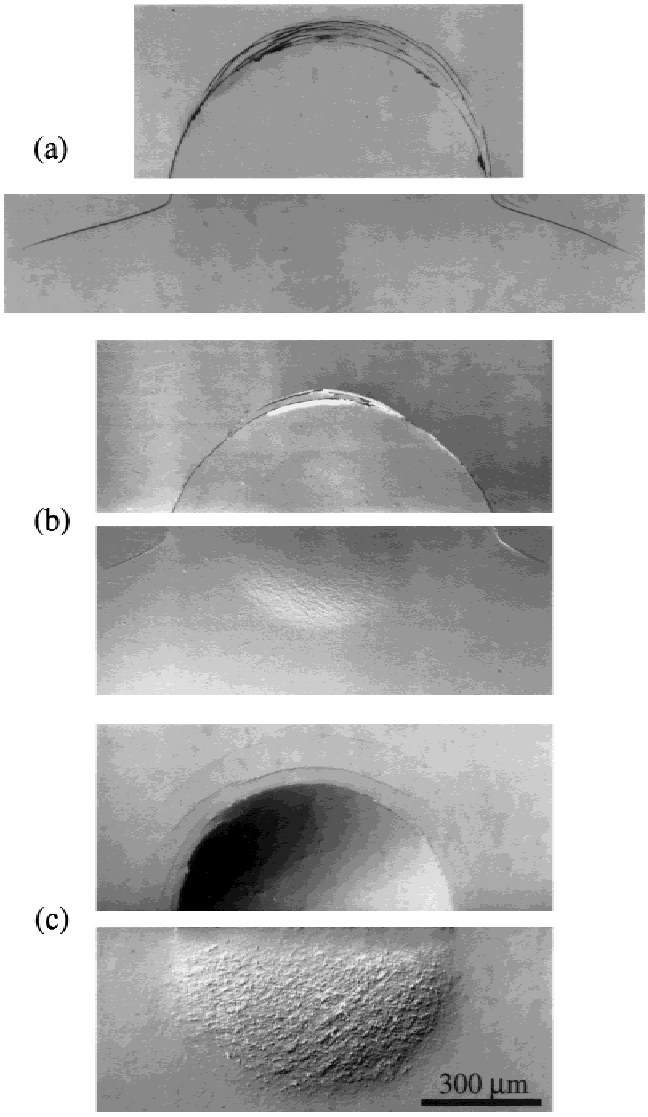

Fig. 10. Hertzian indentation damage in silicon nitride, from tungsten carbide sphere ($r = 1.98$ mm and $P = 4000$ N): (a) F fine, (b) M medium, and (c) C coarse. Half-surface (upper) and section (lower) views from bonded-interface specimens. Optical micrographs, surfaces gold coated after indentation, Nomarski interference. Reproduced from Ref. 81.

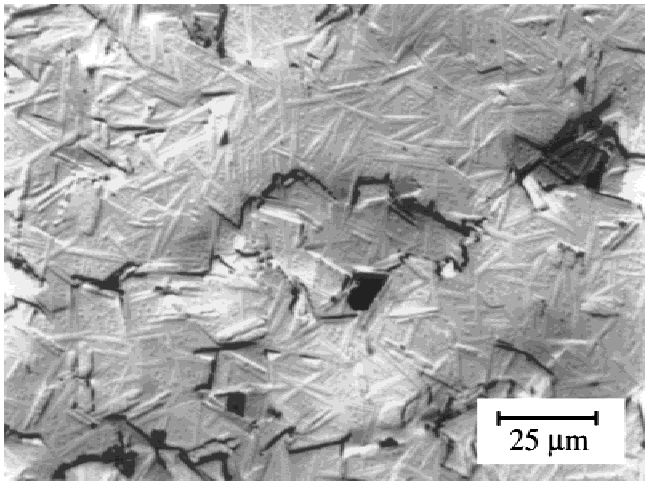

Fig. 11. Enlarged view of subsurface damage microcracks and coalescence in heavily damaged area of Fig. 8(a). Note microfailures at weak interfaces between mica platelets and glass phase. Reproduced from Ref. 32.

by a parameter Nl^3, where N is the number density and l the characteristic size of the composite faults (which, depending on the specific measurement technique, may or may not include both primary fault and secondary microcrack). *In situ* acoustic emission has revealed considerable activity from damage events in heterogeneous silicon carbide, during unloading as well as loading, enabling at least relative measurements of damage intensity.[77] Another nondestructive evaluation (NDE) technique, thermal wave imaging, has been used to provide absolute measurements in alumina and other ceramics (Panel B).

At high loads or large numbers of cycles (Section VI), the damage in the more heterogeneous ceramics can become so intense that neighboring microcracks coalesce (Fig. 11), leading ultimately to extensive material removal. As alluded to earlier, such materials tend to have inferior wear properties.

(2) Damage Mechanics

Macroscopic aspects of the quasi-plastic damage zone beneath a spherical indenter can be confirmed using numerical computational methods, such as the FEM algorithm described in Section II(2). In the FEM calculations, the material below the indenter is allowed to deform in accordance with the bilinear yield relation Eq. (7), using stress–strain data (e.g., Fig. 3) to ''calibrate'' the essential material parameters.[28] Boundaries of the damage zone at any given load are then determined as the shear-stress contour $\tau_{13} = Y/2$. For the glass-ceramic in Fig. 8, the computed contour shows geometrical correspondence with the experimental damage zone. This correspondence confirms that the damage is essentially shear-driven, i.e., is quasi plastic. The FEM computations also demonstrate that the yield can relax the tensile stresses outside the surface contact.[28]

To understand the role of microstructure it is necessary to model the discrete damage events within the confining shear–compression elastic–plastic contact field, Fig. 12(a). The generic picture is that of a closed sliding shear fault with attendant extensile ''wing'' cracks at the constrained fault ends, Fig. 12(b). This type of modeling, while highly phenomenological, has strong precedent in the rock mechanics literature.[17,18,96,97] Because of the compression across the shear fault surfaces the sliding must overcome an internal resistive ''cohesion'' stress τ_c, so that the net sliding shear stress is $\tau_* = \tau_P - \tau_c$, where τ_P is the applied shear stress associated with the applied field. (A more general expression includes an extra friction coefficient μ term, neglected here.[98]) For a body in uniform uniaxial compression containing an array of noninteracting, favorably aligned penny shear faults of number density N and size l (ignoring wing cracks for the moment), we recover the bilinear relation Eq. (7*b*), with[98]

$$Y = 2\tau_c \tag{14a}$$

$$\alpha = 1/(1 + 2Nl^3) \tag{14b}$$

Thus the yield stress Y is determined by the intrinsic shear stress to initiate sliding failure at internal interfaces, and the strain-hardening coefficient α is determined by the damage parameter Nl^3 (with limits $2Nl^3 << 1$ corresponding to a fully elastic response and $2Nl^3 >> 1$ to a fully plastic response). Equation (14) connects the micromechanics with the macroscopic stress–strain curves and opens the way, through N and l, to incorporation of microstructural variables (e.g., grain size and shape, volume fraction of particulate phases) into the analysis.[98]

Extensile wing cracks initiate at the faults above some critical stress, depending on the grain size.[99] (By effectively increasing the fault size, the wing cracks lower α even further than predicted in Eq. (14*b*), leading in extreme cases to ''strain

Panel B. Quantifying Microcrack Damage Using Thermal Wave Imaging

With Lanhua Wei, Therma-Wave, Fremont, California

Several NDE methods exist for detecting contact damage accumulation. Acoustic emission has proved useful in some cases, revealing damage activity during both loading and unloading.[77] Instrumented nanoindenters have been used to probe damage zones on section surfaces (e.g., Fig. 10), and thus to evaluate damage intensities from relations between elastic modulus and microcrack density.[92] One of the more intriguing methods is instrumented thermal wave analysis, which is especially sensitive to the presence of open cracks. The technique can be used in scanning mode to provide a digitized image of the fracture damage distribution, and to quantify the density of microcracks.[93]

Figure B1 shows images of the same alumina specimens as in Fig. 9.[94] High-damage regions are indicated in red (''hot'') and undamaged regions in green (''cold''). The patterns provide a pictorial illustration of the transition from single macrocrack in the fine structures to diffuse microcrack zone in the coarse structures, correlating with the optical observations in Fig. 9.

Quantitative data on crack densities are obtained from evaluations of thermal diffusivities α at each digitized pixel, using a modified version of a relation by Hasselman:[95]

$$Nl^3 = (9/8n) \sum_i^n (\alpha_0/\alpha_i - 1)$$

where α_i is evaluated over all n pixels within the damage zone and α_0 is evaluated without. Figure B2 plots Nl^3 as a function of grain size l. A systematic increase in microcrack damage intensity with microstructural heterogeneity is apparent above a threshold value of l.

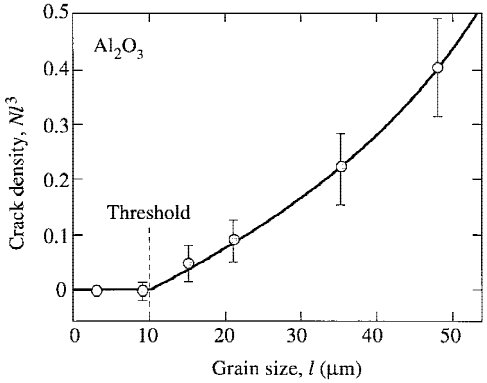

Fig. B2. Microcrack densities in indentation damage zones as function of grain size for alumina materials in Fig. B1. From Ref. 94.

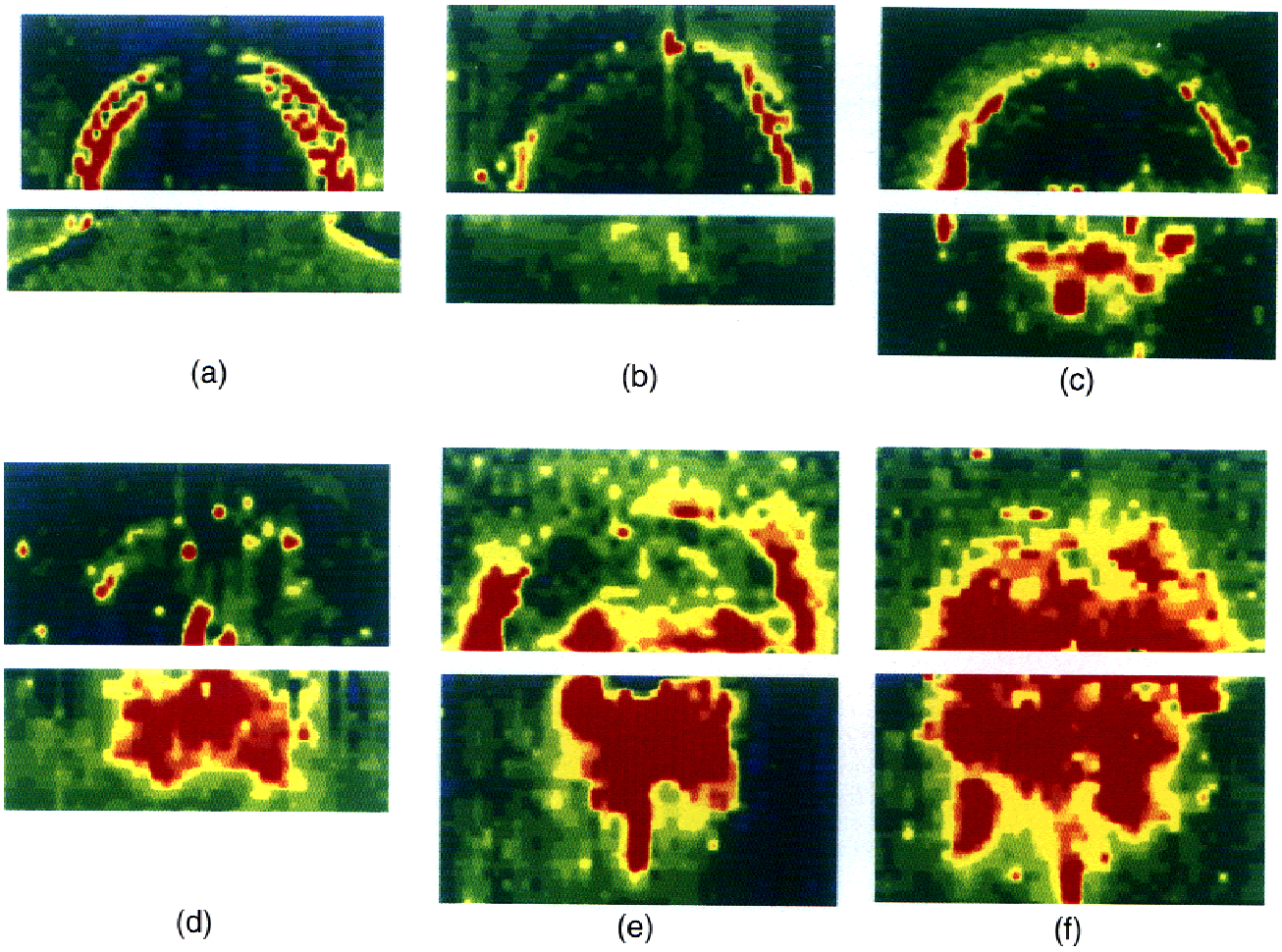

Fig. B1. Thermal wave images of same alumina materials as in Fig. 9. Red designates high crack densities. From Ref. 94.

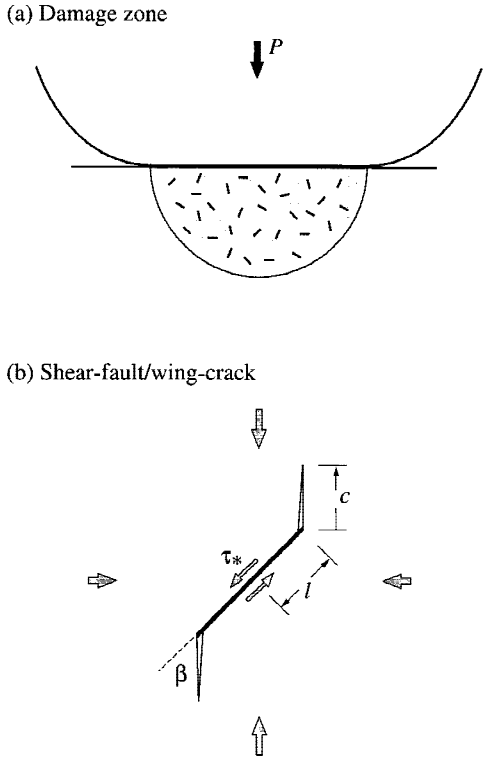

Fig. 12. Schematic of shear-fault/wing-crack system: (a) contact at load P forms array of shear faults within quasi-plastic zone; and (b) individual shear-fault/wing-crack in volume element, treated as pennylike crack with virtual radius $C = c + \gamma l$ and residual shear stress τ_*.

softening.''[98]) Consider an individual penny shear fault of radius l and annular wing crack of width c, with persistent shear stress τ_* in Fig. 12(*b*) (neglecting any reverse sliding during unloading). Following Horii and Nemat-Nasser,[96] the kinked shear-fault/wing-crack can be approximated as a planar penny crack of effective radius

$$C = c + \gamma l \tag{15}$$

where $\gamma \approx 0.27$ is a dimensionless geometry ''correction'' coefficient,[96] acted upon by a residual center-opening force

$$Q = \lambda l^2 \tau_* \tag{16}$$

where λ is another dimensionless coefficient. A residual stress-intensity factor for the wing crack can then be written in familiar form:

$$K = \chi Q / C^{3/2} \tag{17}$$

Equations (15)–(17) provide a functional relation $K = K(c,\tau_*)$.

To connect the stress-intensity factor to the sphere-indentation problem, we need to relate τ_* to contact load P. For the general elastic–plastic contact field this is most practically done empirically, using FEM to compute the maximum shear stress τ_* beneath the indenter at each prescribed load P. From such a procedure we obtain the empirical relation[99]

$$\tau_*(P) = \alpha \tau_c [(P/P_Y)^{1/3} - 1] \tag{18}$$

which yields $K(c,P)$ in Eqs. (15)–(17). Then, imposing the equilibrium condition $K = K_{IC} = T_0$ (now, strictly, short-crack toughness), we can determine $c(P)$.[99] The cracks turn out to be exceedingly difficult to extend even at high loads, reflecting the strong stabilizing influence of the triaxially compressive contact field.[100] Nevertheless, when the loading is extreme (or number of cycles large—see Section VI), coalescence may occur between neighboring faults, signaling ultimate breakdown of the material.

Finally, we have noted the tendency for quasi plasticity in tougher ceramics to be accompanied by suppression of cone cracking. There are two reasons for this: coarser microstructures deflect surface flaws further along weak interfaces, away from tensile stress trajectories into compression regions of the contact field,[81] in a manner analogous to that referred to earlier in connection with large abrasion flaws (Section III(2)); and the onset of yield *below* the contact redistributes and relaxes the tensile stresses *outside* the contact.[28]

V. Strength Degradation from Contact Damage

(1) Experimental Data

A critical issue in designing with ceramics is damage tolerance: if damage does occur, will the component survive subsequent applied stresses? What effect does contact damage have on strength? Such consideration is crucial in many structural applications involving ceramics, e.g., bearings[6,101] and dental restorations.[8] Strength testing also provides a quantitative measure of the damage introduced by the contact event.

The indentation–strength test involves placement of sphere indentations into the centers of prospective tensile surfaces of flexure specimens at specified loads P and contact environments.[65,102–104] Strengths, σ_F, are then measured, usually in four-point or biaxial flexure, and in fast-loading and dry environment to avoid kinetic effects (''inert strengths''). When the damage provides the dominant flaw, the specimens fail from the indentation sites. Illustrative examples are shown in Fig. 13 for the F-, M-, and C-grade silicon nitride represented in Fig. 10.[101] Fractographic examination confirms failures from the bases of cone cracks in the F and M materials, and from within the subsurface damage zones in the C material.

Strengths for the same silicon nitride materials are plotted as functions of load in Fig. 14[101]—the data are experimental strength measurements, the solid curves theoretical fits (Section V(2)). Initially, each material holds its preindented strength with increasing load, corresponding to failures from natural flaws. In the more brittle F-grade silicon nitride ($P_C << P_Y$) and M-grade silicon nitride ($P_C < P_Y$), these strengths suffer abrupt losses at $P = P_C$. On the other hand, in the quasi-plastic C-grade silicon nitride ($P_Y << P_C$), the strengths decrease slowly, and only after some buildup of damage intensity, above $P_D \approx 2P_Y$. These results indicate a superior damage tolerance in the coarser microstructure. However, at very high loads or under fatigue conditions, when cracks coalesce, the quasi-plastic microstructures become subject to accelerated strength losses (Section VI).[99]

Hertzian damage analysis and strength testing are proving a powerful means of characterizing fracture and deformation properties in a broad range of ceramics, including dental ceramics (Panel C).

(2) Modeling

The strength degradation characteristics for indentation-damaged ceramics are calculated from the instability conditions for cone cracks (brittle materials) and shear-fault/wing-cracks (quasi-plastic materials) in uniform tensile fields.[65,99]

(A) Brittle Ceramics: Above the critical load $P = P_C$, failure initiates spontaneously from the base of a cone crack, propagating downward nearly normal to the applied tensile stress. Assuming again a single-valued toughness, $K_{IC} = T_0$ (and ignoring residual stresses from any accompanying quasi plasticity), the classical strength equation applies:

$$\sigma_F = T_0 / \Psi c^{1/2} \tag{19}$$

where Ψ is a crack geometry coefficient (determinable *a priori* from fracture mechanics considerations[65,99]). Combining Eq. (19) with Eqs. (8) and (9) yields $\sigma_F(P)$.

(B) Quasi-plastic Ceramics: Above $P = P_D$, failure initiates from the tip of a wing crack at a discrete shear fault within the diffuse quasi-plastic zone. Recalling the existence of

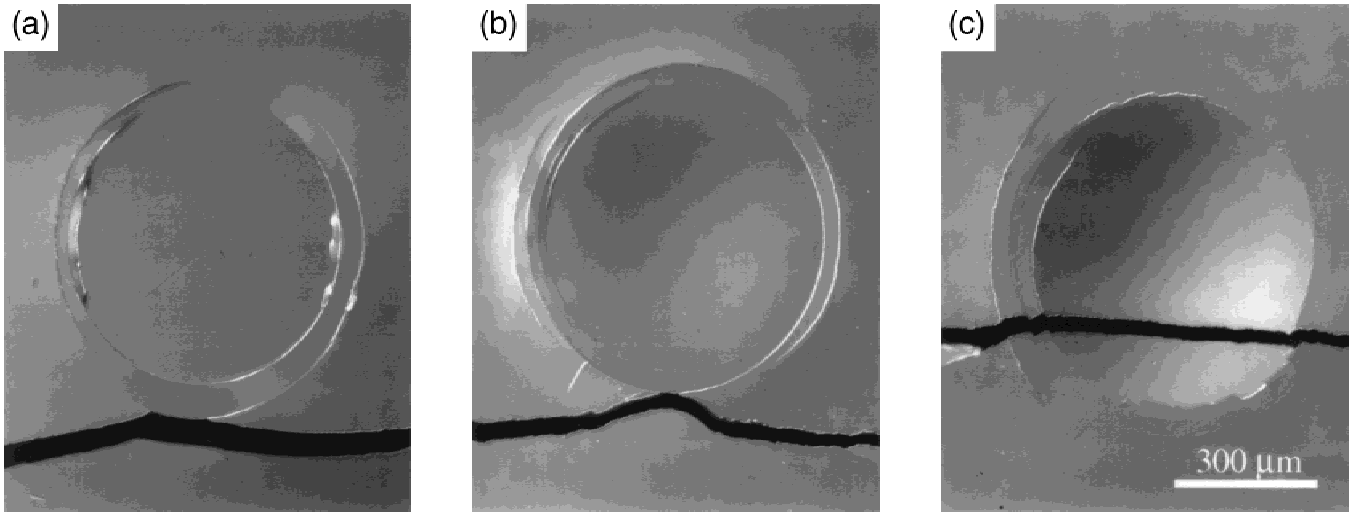

Fig. 13. Surface views of contact failure sites in silicon nitride specimens, from tungsten carbide sphere ($r = 2.38$ mm and $P = 4000$ N): (a) fine-, (b) medium-, and (c) coarse-grade silicon nitride. Surfaces gold coated after indentation, Nomarski interference. Four-point bend-strength specimens, tension axis vertical. From Ref. 101.

the residual driving force on the shear fault in Eq. (17) (but ignoring interactions between neighboring faults), we obtain the stress-intensity factor:

$$K = \chi Q/C^{3/2} + \Psi\sigma C^{1/2} = T_0 \tag{20}$$

(T_0 a short-crack toughness). Combining Eq. (20) with Eqs. (15) and (16), we can show that the wing crack extends stably prior to instability[99] at a failure stress

$$\sigma_F = (3/4\Psi)(T_0^4/4\chi\lambda l^2\tau_*)^{1/3} \tag{21}$$

This equation may then be combined with Eq. (18) to obtain $\sigma_F(P)$.

The solid curves in Fig. 14 represent fits of the theoretical $\sigma_F(P)$ functions to the experimental data.

Conditions for accelerated strength losses due to coalescence of adjacent shear faults at high loads, where neighboring wing cracks merge before attaining their critical dimensions, have also been considered.[99]

VI. Contact Fatigue

Repeated cycling can greatly exacerbate damage in ceramics, especially those with *R*-curves, thereby compromising useful life.[109–111] Mention has already been of the tendency for structural ceramic components such as bearings and dental restorations to fail prematurely in service. Contact fatigue testing with spheres provides a simple means of characterizing the fatigue properties of such ceramics in the critical short-crack domain.[19,78,112,113]

Examples of contact fatigue damage in ceramics are shown in Figs. 15 and 16. Figure 15 compares the surface damage on a moderately coarse alumina (grain size 23 μm)[19] after $n = 1$ and $n = 10$ cycles at the same frequency in water. There is conspicuous enhancement in the damage from cycling. Comparative cycling tests in dry nitrogen show reduced damage accumulation, affirming a chemical influence in the water environments. More tellingly, static tests in water with load held constant over the same time duration as Fig. 15(b) also show reduced damage, indicating that the underlying fatigue effect is nevertheless predominantly mechanical.

Figure 16 compares damage accumulation in two microstructural forms of silicon carbide: homogeneous–brittle (left) and heterogeneous–tough (right).[77,113] In the homogeneous form, cycling causes slight extension of cone cracks, and ultimately detaches a spurious surface collar from the cone mouth. In the heterogeneous form, damage accumulation is much more accelerated, beginning with a barely detectable quasi-plastic zone at $n = 1$ and ending with microcrack coalescence and wholesale surface expulsion of material at $n = 10^6$. Figure 17 is a scanning electron micrograph of the central severe damage zone in this latter case. Note the appearance of copious debris on the surface and attendant voids in the degraded microstructure. The implications concerning the susceptibility to wear are evident.[15,114]

Modeling of contact fatigue is in its infancy. In brittle ceramics, where the fatigue effect is essentially chemical, analysis simply requires the incorporation of an appropriate crack

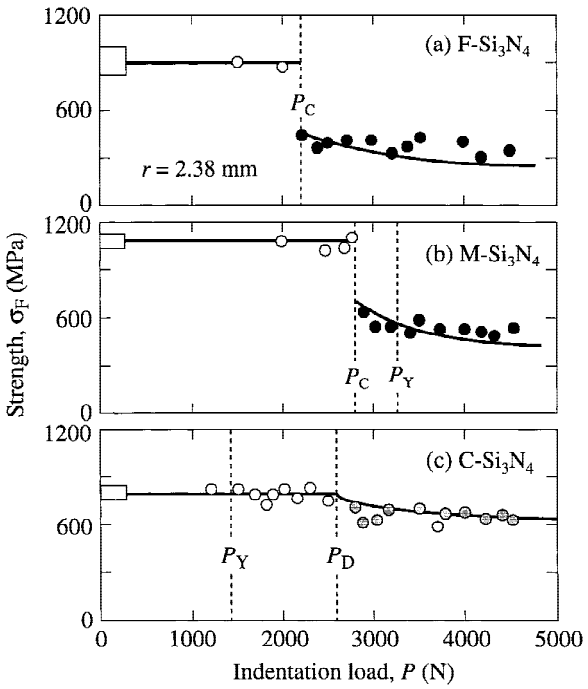

Fig. 14. Strength of silicon nitride specimens indented with tungsten carbide sphere ($r = 2.38$ mm), as function of indentation load. Data points are experimental measurements, indentation tests in air—black symbols represent failures from cone crack origins, gray symbols from quasi-plastic zones, and open symbols from other origins. Solid curves are theoretical fits. Boxes at left axis represent strengths of polished, unindented specimens. Vertical dashed lines indicate critical loads. From Refs. 99 and 101.

Panel C. Dental Ceramics

With Irene Peterson, Materials Science and Engineering Laboratory,
National Institute of Standards and Technology, Gaithersburg, Maryland

Ceramics are increasingly being used in dental restorations, especially in crowns.[105] Unfortunately, current ceramic restorations are susceptible to failure by some form of accumulated damage, from chewing, grinding (''bruxing'') and inadvertent crunching—contact forces in the mouth can easily exceed 200 N, over cuspal radii of 2–4 mm. Durability, wear, and fatigue resistance are key mechanical issues, if subordinate to aesthetics (or even to cost and ease in preparation), in design considerations. Contact with spherical indenters offers a simple route to characterization of dental materials, under conditions that closely simulate oral function.[8]

The first quantities of interest are the critical loads to induce damage in the ceramic surface. Figure C1 plots the loads P_C (Fig. C1(a)) and P_Y (Fig. C1(b)) for cone cracking and yield as a function of sphere radius in three selected generic dental materials:[8] porcelain, micaceous glass-ceramic (analogous to the material in Fig. 8 but smaller mica platelet size), and glass-infiltrated alumina. Both $P_C(r)$ and $P_Y(r)$ increase monotonically, in approximate linear (Section III) and quadratic (Section IV) manner, respectively. The shaded boxes indicate the domain of oral forces and cuspal radii referred to above. The alumina–glass has the highest resistance to cracking, the porcelain the highest resistance to quasi plasticity. However, it is evident that all of the materials are vulnerable to some form of damage during severe contact, especially from spurious sharp objects and from sustained cyclic loading.

The next question is the survivability of a material once damage does occur. Figure C2 shows strength degradation plots (Section V) for the same three monolithic materials as above. Both porcelain and glass-ceramic fail from cone cracks above a critical load, whereas alumina–glass fails predominantly (but not exclusively) from quasi-plastic zones.[106] The porcelain is particularly weak and brittle. Unfortunately, the comparatively high strength properties of the alumina–glass are negated somewhat by inferior aesthetics, necessitating a porcelain veneer.

Indentation–strength tests establish a base for systematic investigation of the crucial role of microstructure in damage tolerance. Strength data on a range of glass-ceramics crystallized at increasing heat-treatment temperatures, with corresponding increasing microstructural scale, are plotted in Fig. C3.[107] Results are shown for surfaces broken after fine polishing (''pristine'') and after damage by sphere indentation (''indented''). Whereas the pristine strengths decrease steadily with microstructural scale, those after indentation pass through a maximum as first cone cracking is suppressed then quasi plasticity proliferates. Note the ever-diminishing differential between the two curves in the coarser microstructures. Of these microstructures, that crystallized at or about 1040°C appears to offer an optimum combination of high strength and damage tolerance—this is the microstructure represented in Figs. C1 and C2 and that most closely resembles commercially available dental glass-ceramics.[107]

In actual crowns, dental ceramics are often configured in ''veneer/core'' layers. The lesson from natural teeth is that such combinations can produce extraordinarily resilient, damage tolerant structures,[105] with complex but stable crack patterns (cf. Fig. 19(c)). Contact studies of damage patterns in simulated dental layer structures are under way.[108]

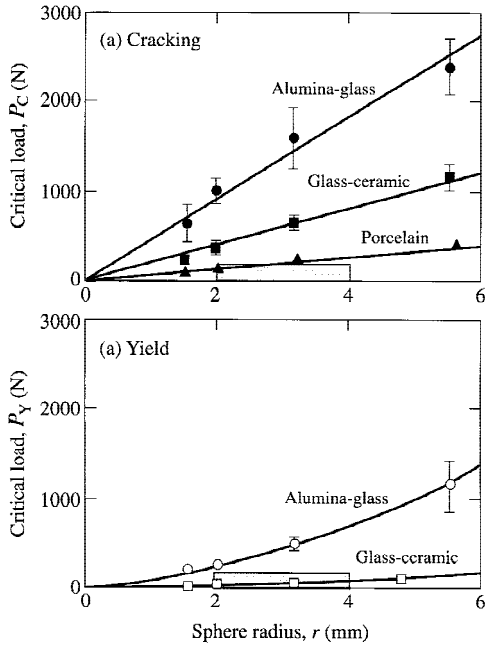

Fig. C1. Critical load functions $P_C(r)$ and $P_Y(r)$ for generic dental ceramics, for indentations with tungsten carbide spheres. Shaded box designates domain of typical dental function. Some data replotted from Ref. 8.

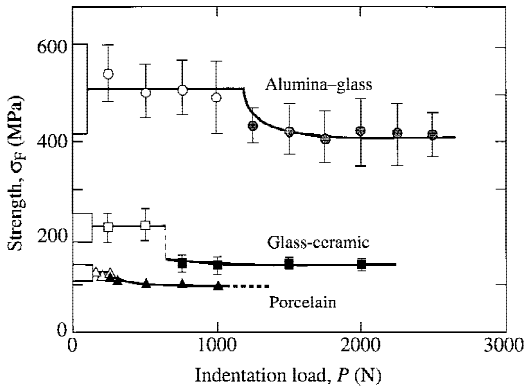

Fig. C2. Strength as function of contact load for same dental ceramics as in Fig. C1, for indentations with tungsten carbide sphere (r = 3.18 mm). Some data replotted from Ref. 8.

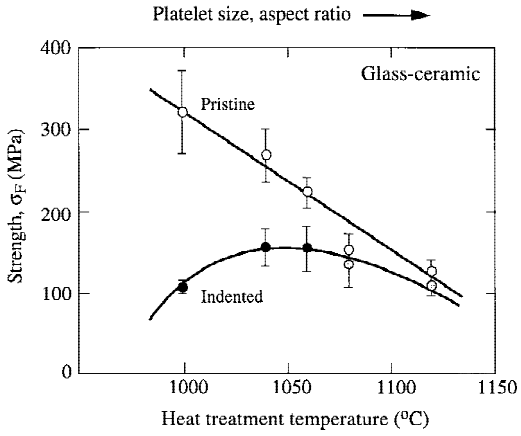

Fig. C3. Strengths of micaceous glass-ceramics as function of mica platelet size. Data for pristine (unindented) surfaces (open circles), and contact-damaged surfaces (tungsten carbide sphere, r = 3.18 mm, and P = 750 N)—black symbols represent failures from cone cracks, gray symbols failures from quasi-plastic zones, open symbols from other origins. Data courtesy A. Pajares and Y-G. Jung.

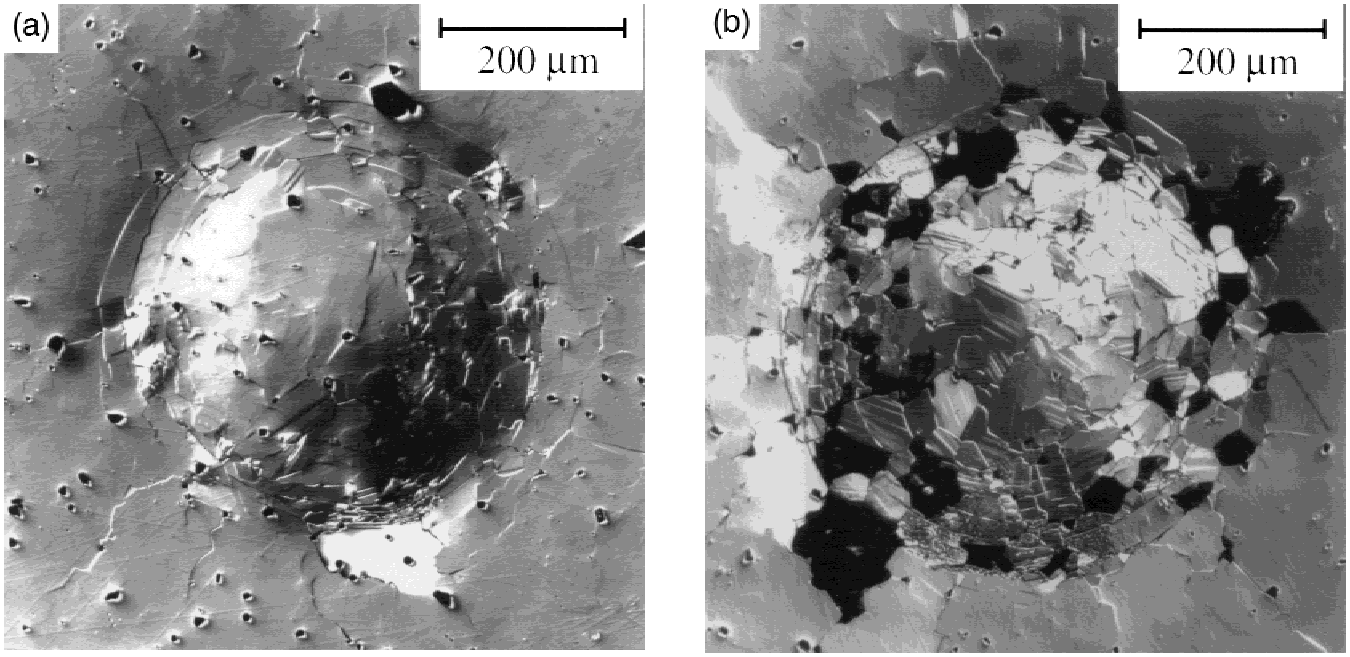

Fig. 15. Indentation damage in coarse alumina ($l = 23$ μm) from tungsten carbide sphere ($r = 1.98$ mm and $P = 2000$ N—cf. $P_Y \approx 1000$ N) at 0.002 Hz, in water: (a) $n = 1$ and (b) $n = 10$ cycles. Surfaces gold coated after indentation, Nomarski interference. From Ref. 19.

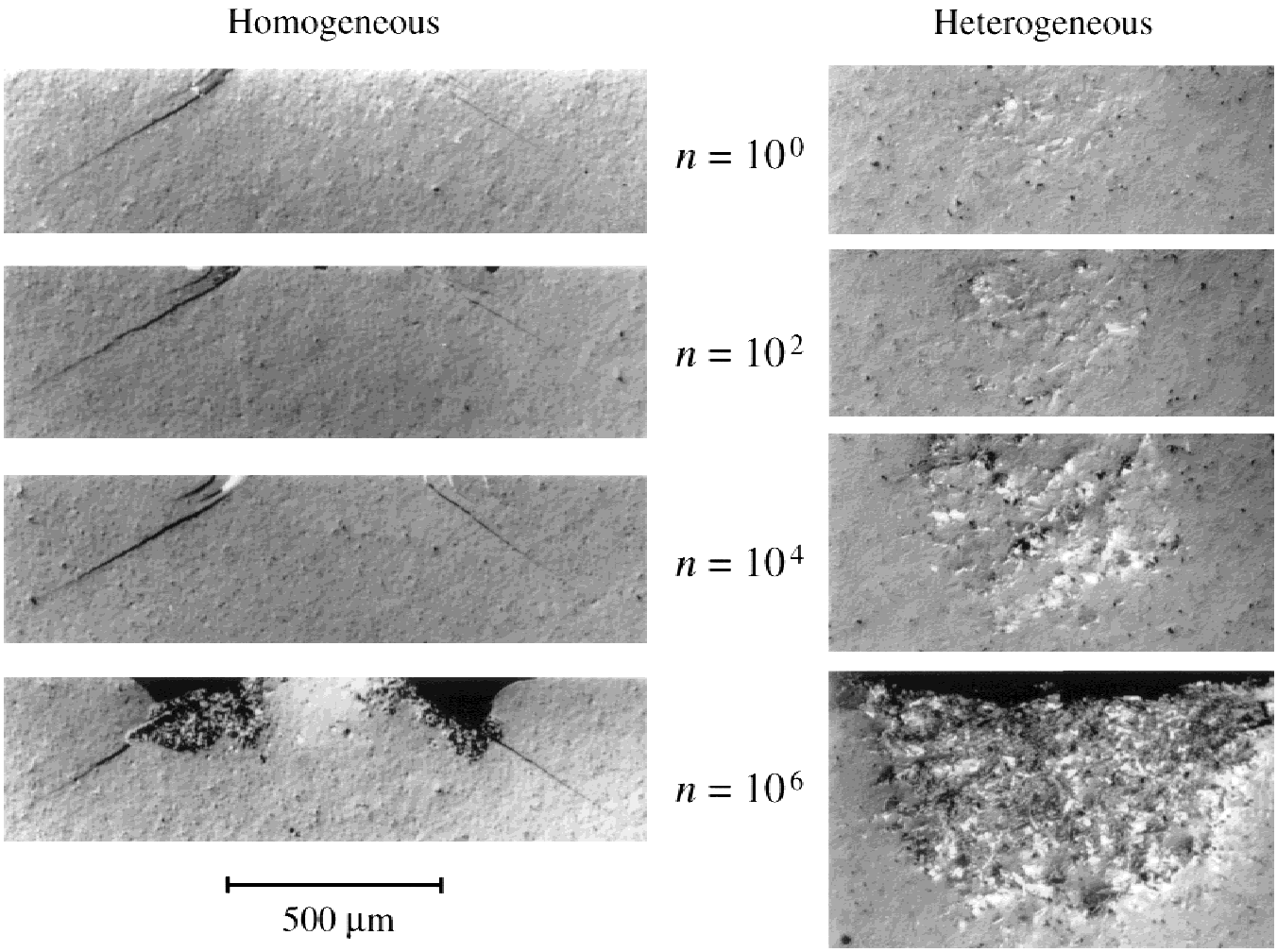

Fig. 16. Section views of Hertzian contact sites in brittle (homogeneous) and tough (heterogeneous) silicon carbide, from tungsten carbide sphere ($r = 3.18$ mm, $P = 1000$ N, and $f = 10$ Hz), in air. Bonded-interface specimens, surfaces gold coated after indentation, Nomarski interference. From Ref. 113.

velocity relation $v = v(K)$ into the cone fracture mechanics.[113] In quasi-plastic ceramics, mechanical processes dominate—damage accumulates primarily by decremental attrition at the sliding shear fault interfaces (Fig. 17). This attrition is manifested as a progressive reduction in the frictional sliding resistance at successive cycles, i.e., in the cohesion term τ_c (and/or μ terms),[115,116] effectively diminishing the yield stress in Eq. (14*a*). Complex interactions between chemical and mechanical effects can occur (e.g., by reducing the friction at shear faults and enhancing the extension of wing cracks), although these micro-interactions are not yet well understood. Macroscopic friction between the indenter and specimen can cause additional surface ''fretting.''[21,117]

Contact fatigue is quantifiable by its effect on strength, $\sigma_F(n)$, at given load P. Figure 18 shows strength data for the same silicon nitrides considered earlier (Fig. 10), for a load well below the single-cycle thresholds for cone cracks (P_C) in F-grade silicon nitride and M-grade silicon nitride and for quasi plasticity (P_D) in C-grade silicon nitride. As with the single-cycle $\sigma_F(P)$ curves (Fig. 14), the strengths for F- and M-grade silicon nitride are abruptly degraded at some critical value of n, whereas the degradation in C-grade silicon nitride is more continuous above the critical n. However, note the very rapid decrease in strengths of C-grade silicon nitride at very large n, signaling the end of the useful life of this material.

It is apparent from Figs. 16–18 that quasi-plastic ceramics are more susceptible to fatigue than their brittle counterparts. What makes the quasi-plastic damage mode especially insidious is the difficulty of detection and screening in its early stages. In ceramics where the competition between fracture and deformation is finely balanced, it is possible for the failure mode to change from brittle in single-cycle loading to quasi plastic in multi-cycling loading, making any predictions of fatigue responses from static test data especially suspect.

VII. Layer Structures

Finally, we indicate how current contact testing is contributing to a new design philosophy for ceramic-based layer structures. We have seen how microstructural weakening and coarsening, while improving long-crack toughness, tend to degrade strength and wear resistance. A potential way of averting compromise in design is to tailor laminates with hard/brittle outer (''protective'') layers and soft/tough inner (''functional'') layers. In principle, such layer systems should exhibit both high wear resistance and high toughness, with reduced susceptibility to strength degradation from damage accumulation. Critical

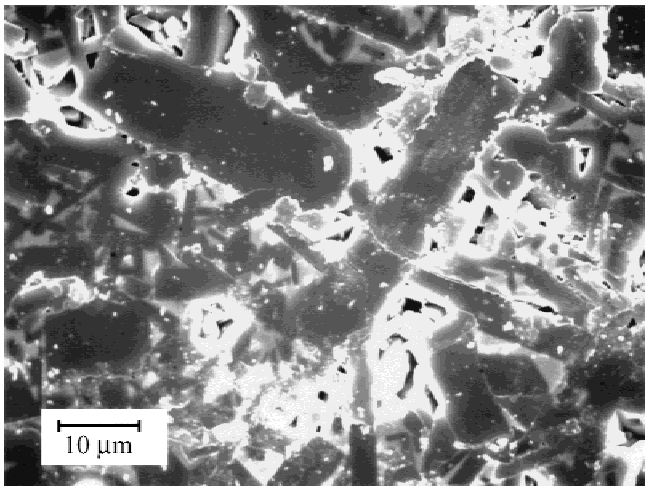

Fig. 17. Scanning electron micrograph of Hertzian cyclic-contact damage in heterogeneous silicon carbide, from center region of subsurface damage zone at $n = 10^6$ in Fig. 16. Note sliding-interface debris and surface cavities from material removal. From Ref. 113.

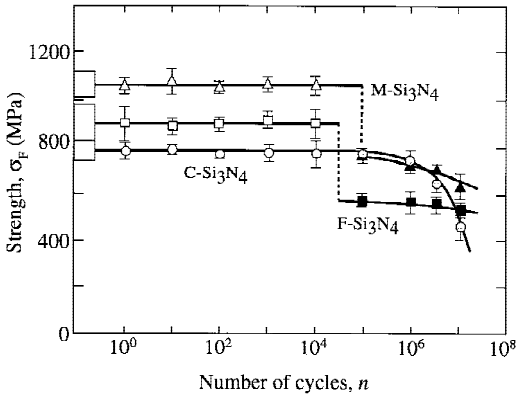

Fig. 18. Strength of silicon nitride specimens indented with tungsten carbide sphere ($r = 1.98$ mm and $P = 1000$ N) as function of number of contact cycles at $f = 10$ Hz, demonstrating fatigue. Data points are experimental measurements, indentation tests in air—black symbols represent failures from cone cracks, gray symbols failures from quasi-plastic zones, and open symbols from other origins. Boxes at left axis represent strengths of polished, unindented specimens. Data courtesy S. K. Lee.

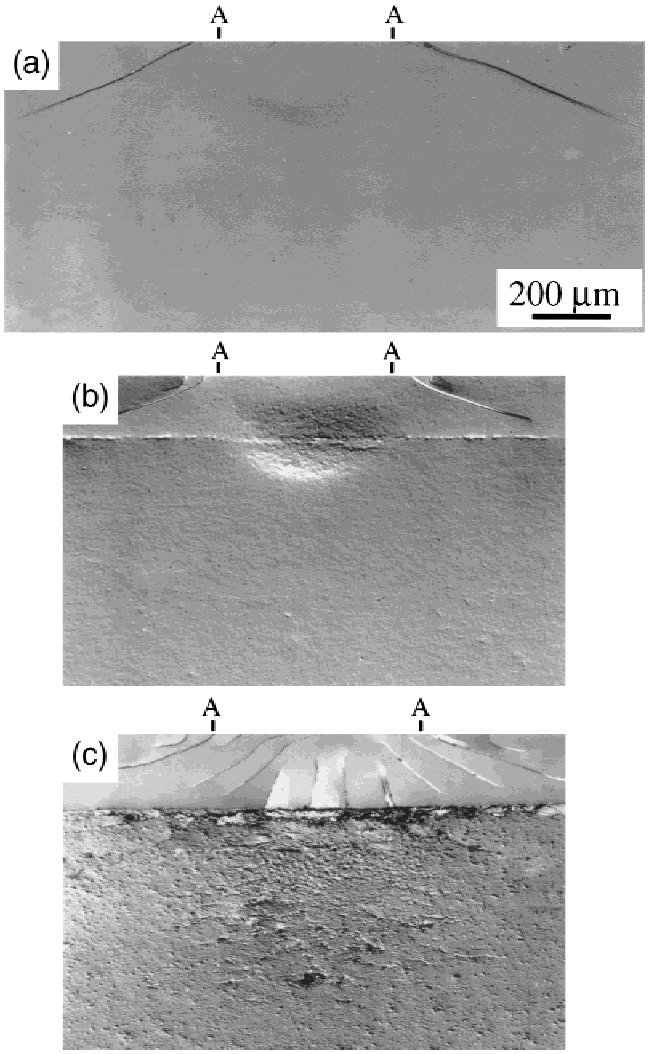

Fig. 19. Section views of Hertzian contact damage in silicon nitride bilayers, using tungsten carbide sphere ($r = 1.98$ mm and $P = 3000$ N): (a) monolith of fine-grain material, showing fully developed cone crack with barely detectable subsurface quasi plasticity; (b) bilayer of fine-grain coating on coarse-grain substrate; and (c) similar, but on substrate with 30% boron nitride additive. Bonded-interface specimens, Nomarski optical micrographs. Contact diameter AA indicated. From Ref. 123.

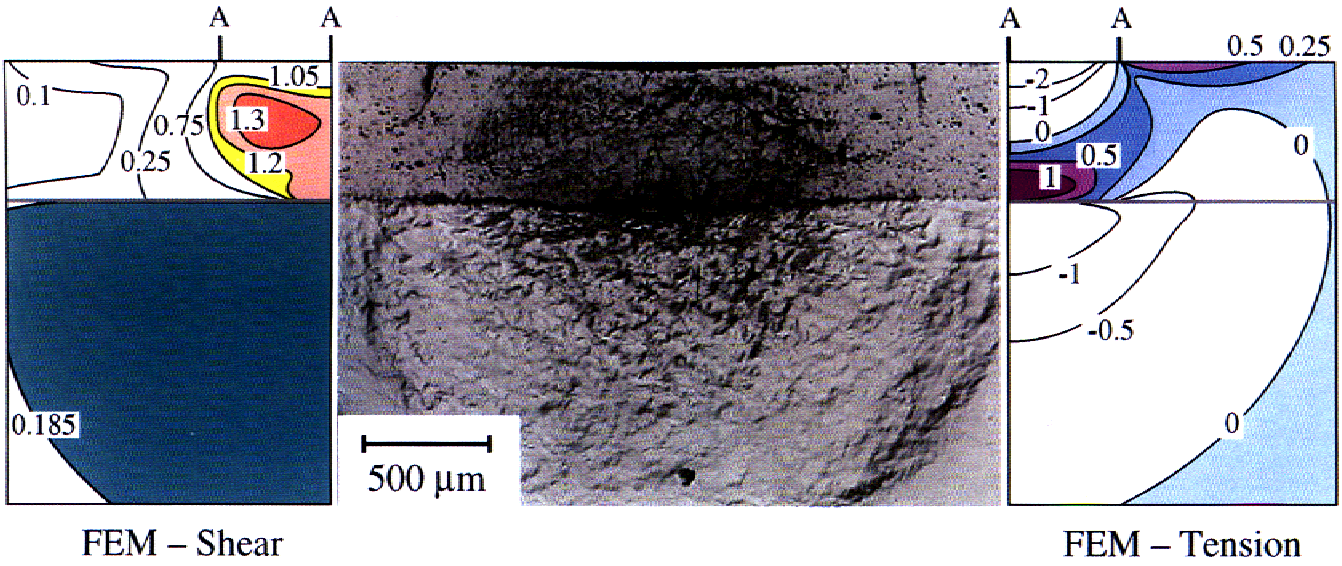

Fig. 20. Section view of Hertzian contact damage in plasma-sprayed alumina–40% titania coating on mild steel substrate, from tungsten carbide sphere ($r = 3.18$ mm and $P = 1500$ N). Note correspondence between locations of coating cracks and principal tensile stresses (right), and between yield zones and principal shear stresses in both coating and substrate (left). From Ref. 127.

elements of the new philosophy are: (i) incorporation of strong rather than weak interlayer interfaces, to avoid delamination; (ii) adjustment of elastic–plastic mismatch between layers so as to partition energy from the contact loading system into competing fracture and quasi-plastic modes, and thus to suppress (rather than deflect) any cone (or other) cracks that originate in the outer layers. This philosophy has been demonstrated on several material systems: ceramic bilayers, alumina/alumina,[84,118,119] glass/glass-ceramic,[120] and silicon nitride/silicon nitride;[121–123] thermal barrier coatings;[124–128] and simulated dental structures.[108] We briefly describe two examples here.

Our first example, Fig. 19, shows sphere indentations in two silicon nitride bilayers with a common homogeneous top layer (''coating'') on two heterogeneous underlayers with quite different toughness properties (''substrates'').[123] In its bulk state (Fig. 19(a)), the coating is a relatively fine silicon nitride (cf. Fig. 10(a)) with well-developed cone fracture. The substrate in the first bilayer (Fig. 19(b)) is a coarse but pure silicon nitride (cf. Fig. 10(c)), corresponding to modest coating/substrate elastic–plastic mismatch. A cone fracture is still evident, but is significantly shallower. Note the appearance of a deformation zone beneath the indenter. The substrate in the second bilayer (Fig. 19(c)) has a much more heterogeneous microstructure, with incorporated boron nitride platelets as a softening phase,[122] corresponding to a large coating/substrate elastic–plastic mismatch. The damage pattern is much more complex, with multiple transverse coating fractures extending both downward from the top surface and upward from the interlayer interface. Substrate yield is now pronounced. It is noteworthy that the transverse cracks remain fully contained with the coating in both bilayers—extreme loads are needed to drive these cracks through the coating thickness and cause failure—and that there is no substantial delamination at the interlayer interface. It is clear that the mismatch has a profound influence on the coating fracture, attesting to the damage tolerance of these structures.

Our second example concerns a plasma-sprayed alumina–titania coating on a mild steel substrate.[127] Such coatings are notorious for their extreme defect and pore content.[129] Figure 20 shows indentation damage in this system. Intense diffuse microcracking and yield in the substrate are observed. However, macroscopic cracking is limited: some delamination has occurred at the interlayer interface, but transverse cracks are conspicuously small. FEM analyses of tension and shear stress distributions provide correlations with these observed macroscopic cracking and yield patterns.[127] Thus, despite the wholesale damage intensity, the system remains essentially intact. The charm of these coatings is in the very defect complexion that facilitates the damage, dissipating and redistributing mechanical energy beneath the contact, resulting in exceptional damage tolerance as well as in other desirable (e.g., thermal resistance[129]) properties.

Contact mechanics of ceramic-based layer material systems from sphere indentations constitutes a relatively new area of research. Damage modes and geometries are still being identified, at both the macroscopic (above) and microscopic[130] levels, and the roles of elastic mismatch and interfacial bonding are being elucidated.[128] Analyses of elastic–plastic stress fields[108,126,131,132] and of indentation stress–strain curves[133] are being developed. Extensions of contact theory and experiment to multilayer[134] and graded structures are being reported.[135] The legacy of Hertz appears poised to survive well into the next century of ceramics research.

Acknowledgments: The author expresses deep gratitude to the many students, colleagues, and friends, too numerous to list here, whose critical contributions are represented in this article.

References

[1]H. Hertz, *Hertz's Miscellaneous Papers*; Chs. 5 and 6. Macmillan, London, U.K., 1896.
[2]B. R. Lawn and T. R. Wilshaw, ''Indentation Fracture: Principles and Applications,'' *J. Mater. Sci.*, **10** [6] 1049–81 (1975).
[3]B. R. Lawn, *Fracture of Brittle Solids*; Ch. 8. Cambridge University Press, Cambridge, U.K., 1993.
[4]D. Tabor, *Hardness of Metals.* Clarendon, Oxford, U.K., 1951.
[5]R. F. Cook and G. M. Pharr, ''Direct Observation and Analysis of Indentation Cracking in Glasses and Ceramics,'' *J. Am. Ceram. Soc.*, **73** [4] 787–817 (1990).
[6]R. N. Katz and J. G. Hannoosh, ''Ceramics for High-Performance Rolling Element Bearings: A Review and Assessment,'' *Int. J. High Technol. Ceram.*, **1**, 69–79 (1985).
[7]D. W. Richerson, *Modern Ceramic Engineering.* Marcel Dekker, New York, 1992.
[8]I. M. Peterson, A. Pajares, B. R. Lawn, V. P. Thompson, and E. D. Rekow, ''Mechanical Characterization of Dental Ceramics Using Hertzian Contacts,'' *J. Dent. Res.*, **77** [4] 589–602 (1998).
[9]B. R. Lawn and D. B. Marshall, ''Mechanisms of Micro-Contact in Brittle Solids''; pp. 63–82 in *Lithic Use-Wear.* Edited by B. Hayden. Academic, New York, 1979.
[10]F. Auerbach, ''Measurement of Hardness,'' *Ann. Phys. Chem.*, **43**, 61 (1891).
[11]F. C. Frank and B. R. Lawn, ''On the Theory of Hertzian Fracture,'' *Proc. R. Soc. London*, **A299** [1458] 291–306 (1967).

[12]R. Knehans and R. Steinbrech, ''Memory Effect of Crack Resistance During Slow Crack Growth in Notched Al_2O_3 Bend Specimens,'' *J. Mater. Sci. Lett.*, **1** [8] 327–29 (1982).

[13]P. L. Swanson, C. J. Fairbanks, B. R. Lawn, Y.-W. Mai, and B. J. Hockey, ''Crack–Interface Grain Bridging as a Fracture Resistance Mechanism in Ceramics: I. Experimental Study on Alumina,'' *J. Am. Ceram. Soc.*, **70** [4] 279–89 (1987).

[14]R. W. Steinbrech, A. Reichl, and W. Schaarwächter, ''*R*-Curve Behavior of Long Cracks in Alumina,'' *J. Am. Ceram. Soc.*, **73** [7] 2009–15 (1990).

[15]S.-J. Cho, B. J. Hockey, B. R. Lawn, and S. J. Bennison, ''Grain-Size and *R*-Curve Effects in the Abrasive Wear of Alumina,'' *J. Am. Ceram. Soc.*, **72** [7] 1249–52 (1989).

[16]B. R. Lawn, N. P. Padture, H. Cai, and F. Guiberteau, ''Making Ceramics 'Ductile','' *Science* (*Washington, D.C.*), **263**, 1114–16 (1994).

[17]J. C. Jaeger and N. G. W. Cook, *Fundamentals of Rock Mechanics*; Chs. 3 and 12. Chapman and Hall, London, U.K., 1971.

[18]M. S. Paterson, *Experimental Rock Deformation—The Brittle Field*. Springer-Verlag, Berlin, Germany, 1978.

[19]F. Guiberteau, N. P. Padture, H. Cai, and B. R. Lawn, ''Indentation Fatigue: A Simple Cyclic Hertzian Test for Measuring Damage Accumulation in Polycrystalline Ceramics,'' *Philos. Mag. A*, **68** [5] 1003–16 (1993).

[20]S. Timoshenko and J. N. Goodier, *Theory of Elasticity*; Ch. 13. McGraw-Hill, New York, 1951.

[21]K. L. Johnson, *Contact Mechanics*. Cambridge University Press, London, U.K., 1985.

[22]M. V. Swain and B. R. Lawn, ''A Study of Dislocation Arrays at Spherical Indentations in LiF as a Function of Indentation Stress and Strain,'' *Phys. Status Solidi*, **35** [2] 909–23 (1969).

[23]M. T. Huber, ''Zur Theorie der Berührung Fester Elasticher Körper,'' *Ann. Phys.* (*Leipzig*), **43** [61] 153–63 (1904).

[24]G. M. Hamilton and L. E. Goodman, ''The Stress Field Created by a Circular Sliding Contact,'' *J. Appl. Mech.*, **33**, 371–76 (1966).

[25]G. M. Hamilton, ''Explicit Equations for the Stresses Beneath a Sliding Spherical Contact,'' *Proc. Inst. Mech. Eng.*, **197C**, 53–59 (1983).

[26]R. Hill, *The Mathematical Theory of Plasticity*. Oxford University Press, London, U.K., 1950.

[27]A. C. Fischer-Cripps, ''Elastic–Plastic Behaviour in Materials Loaded With a Spherical Indenter,'' *J. Mater. Sci.*, **32**, 727–36 (1997).

[28]A. C. Fischer-Cripps and B. R. Lawn, ''Stress Analysis of Contact Deformation in Quasi-Plastic Ceramics,'' *J. Am. Ceram. Soc.*, **79** [10] 2609–18 (1996).

[29]M. V. Swain and J. T. Hagan, ''Indentation Plasticity and the Ensuing Fracture of Glass,'' *J. Phys. D: Appl. Phys.*, **9**, 2201–14 (1976).

[30]C. K. Chyung, G. H. Beall, and D. G. Grossman, ''Microstructures and Mechanical Properties of Mica Glass-Ceramics''; pp. 1167–94 in *Electron Microscopy and Structure of Materials*. Edited by G. Thomas, R. M. Fulrath, and R. M. Fisher. University of California Press, Berkeley, CA, 1972.

[31]K. Chyung, G. H. Beall, and D. G. Grossman, ''Fluorophlogopite Mica Glass-Ceramics''; pp. 33–40 in *Proceedings of 10th International Glass Congress*, No. 14. Edited by M. Kunugi, M. Tashiro, and N. Saga. The Ceramic Society of Japan, Kyoto, Tokyo, Japan, 1974.

[32]H. Cai, M. A. Stevens Kalceff, and B. R. Lawn, ''Deformation and Fracture of Mica-Containing Glass-Ceramics in Hertzian Contacts,'' *J. Mater. Res.*, **9** [3] 762–70 (1994).

[33]J. P. Tillett, ''Fracture of Glass by Spherical Indenters,'' *Proc. Phys. Soc. London*, **B69** [433] 47–54 (1956).

[34]F. C. Roesler, ''Brittle Fractures Near Equilibrium,'' *Proc. Phys. Soc. London*, **B69**, 981–92 (1956).

[35]F. C. Roesler, ''Indentation Hardness of Glass as an Energy Scaling Law,'' *Proc. Phys. Soc. London*, **B69** [433] 55–60 (1956).

[36]V. R. Howes and S. Tolansky, ''Pressure Crack Figures on Diamond Faces: I. The Octahedral Face,'' *Proc. R. Soc. London*, **A230**, 287–93 (1955).

[37]V. R. Howes and S. Tolansky, ''Pressure Crack Figures on Diamond Faces: II. The Dodecahedral and Cubic Faces,'' *Proc. R. Soc. London*, **A230**, 294–301 (1955).

[38]S. Tolansky and V. R. Howes, ''Induction of Ring Cracks on Diamond Surfaces,'' *Proc. Phys. Soc. London*, **B70**, 521–26 (1957).

[39]B. R. Lawn and H. Komatsu, ''The Nature of Deformation Around Pressure Cracks on Diamond,'' *Philos. Mag.*, **14** [130] 689–99 (1966).

[40]O. W. Johnson, ''Damage Produced in Ge at Room Temperature by Indentation,'' *J. Appl. Phys.*, **37** [7] 2521–26 (1966).

[41]B. R. Lawn, ''Hertzian Fracture in Single Crystals with the Diamond Structure,'' *J. Appl. Phys.*, **39** [10] 4828–36 (1968).

[42]G. I. Barenblatt, ''The Mathematical Theory of Equilibrium Cracks in Brittle Fracture,'' *Adv. Appl. Mech.*, **7**, 55–129 (1962).

[43]J. S. Williams, B. R. Lawn, and M. V. Swain, ''Cone Crack Closure in Brittle Solids,'' *Phys. Status Solidi A*, **2**, 7–29 (1970).

[44]K. Peter, ''Sprödbruch und Mikroplastizität von Glas in Eindruckversuchen,'' *Glasstech. Ber.*, **37** [7] 333–45 (1964).

[45]B. R. Lawn, T. Jensen, and A. Arora, ''Brittleness as an Indentation Size Effect,'' *J. Mater. Sci.*, **11** [3] 573–75 (1976).

[46]B. R. Lawn and D. B. Marshall, ''Hardness, Toughness, and Brittleness: An Indentation Analysis,'' *J. Am. Ceram. Soc.*, **62** [7–8] 347–50 (1979).

[47]K. E. Puttick, ''Energy Scaling, Size Effects, and Ductile–Brittle Transitions in Fracture,'' *J. Phys. D: Appl. Phys.*, **12**, L19–L23 (1979).

[48]A. S. Argon, ''Distribution of Cracks on Glass Surfaces,'' *Proc. R. Soc. London*, **A250**, 482–92 (1959).

[49]H. L. Oh and I. Finnie, ''The Ring Cracking of Glass by Spherical Indenters,'' *J. Mech. Phys. Solids*, **15**, 401–11 (1967).

[50]F. B. Langitan and B. R. Lawn, ''Hertzian Fracture Experiments on Abraded Glass Surfaces as Definitive Evidence for an Energy Balance Explanation of Auerbach's Law,'' *J. Appl. Phys.*, **40** [10] 4009–17 (1969).

[51]C. J. Culf, ''Fracture of Glass Under Various Liquids and Gases,'' *J. Soc. Glass Technol.*, **41**, 157T–167T (1957).

[52]M. V. Swain and B. R. Lawn, ''A Microprobe Technique for Measuring Slow Crack Velocities in Brittle Solids,'' *Int. J. Fact. Mech.*, **9** [4] 481–83 (1973).

[53]R. Mouginot and D. Maugis, ''Fracture Indentation Beneath Flat and Spherical Punches,'' *J. Mater. Sci.*, **20**, 4354–76 (1985).

[54]F. B. Langitan and B. R. Lawn, ''Effect of a Reactive Environment on the Hertzian Strength of Brittle Solids,'' *J. Appl. Phys.*, **41** [8] 3357–65 (1970).

[55]A. G. Mikosza and B. R. Lawn, ''Section-and-Etch Study of Hertzian Fracture Mechanics,'' *J. Appl. Phys.*, **42** [13] 5540–45 (1971).

[56]J. S. Nadeau and A. S. Rao, ''Hertzian Fracture of a Lithium Silicate Glass and Glass-Ceramic,'' *J. Can. Ceram. Soc.*, **41**, 63–67 (1972).

[57]J. S. Nadeau, ''Hertzian Fracture of Vitreous Carbon,'' *J. Am. Ceram. Soc.*, **56** [9] 467–72 (1973).

[58]M. T. Laugier, ''Hertzian Fracture of Sintered Alumina,'' *J. Mater. Sci.*, **19**, 254–58 (1984).

[59]M. T. Laugier, ''Toughness Determination of Some Ceramic Tool Materials Using the Method of Hertzian Indentation Fracture,'' *J. Mater. Sci. Lett.*, **4**, 1542–44 (1985).

[60]H. Matzke and R. Warren, ''Hertzian Crack Growth in ThO_2 Observed by Serial Sectioning,'' *J. Mater. Sci. Lett.*, **1**, 441–44 (1982).

[61]K. Zeng, K. Breder, and D. J. Rowcliffe, ''The Hertzian Stress Field and Formation of Cone Cracks: I. Theoretical Approach,'' *Acta Metall.*, **40** [10] 2595–600 (1992).

[62]K. Zeng, K. Breder, and D. J. Rowcliffe, ''The Hertzian Stress Field and Formation of Cone Cracks: II. Determination of Fracture Toughness,'' *Acta Metall.*, **40** [10] 2601–605 (1992).

[63]P. D. Warren, ''Determining the Fracture Toughness of Brittle Materials by Hertzian Indentation,'' *J. Eur. Ceram. Soc.*, **15**, 201–207 (1995).

[64]B. R. Lawn, T. R. Wilshaw, and N. E. W. Hartley, ''A Computer Simulation Study of Hertzian Cone Crack Growth,'' *Int. J. Fract.*, **10** [1] 1–16 (1974).

[65]B. R. Lawn, S. M. Wiederhorn, and H. Johnson, ''Strength Degradation of Brittle Surfaces: Blunt Indenters,'' *J. Am. Ceram. Soc.*, **58** [9–10] 428–32 (1975).

[66]N. E. W. Hartley and T. R. Wilshaw, ''Deformation and Fracture of Synthetic α-Quartz,'' *J. Mater. Sci.*, **8**, 265–78 (1973).

[67]M. V. Swain, J. S. Williams, B. R. Lawn, and J. J. H. Beek, ''A Comparative Study of the Fracture of Various Silica Modifications Using the Hertzian Test,'' *J. Mater. Sci.*, **8** [8] 1153–64 (1973).

[68]A. G. Evans and E. A. Charles, ''Fracture Toughness Determinations by Indentation,'' *J. Am. Ceram. Soc.*, **59** [7–8] 371–72 (1976).

[69]G. R. Anstis, P. Chantikul, D. B. Marshall, and B. R. Lawn, ''A Critical Evaluation of Indentation Techniques for Measuring Fracture Toughness: I. Direct Crack Measurements,'' *J. Am. Ceram. Soc.*, **64** [9] 533–38 (1981).

[70]T. R. Wilshaw, ''The Hertzian Fracture Test,'' *J. Phys. D: Appl. Phys.*, **4** [10] 1567–81 (1971).

[71]A. C. Fischer-Cripps and R. E. Collins, ''The Probability of Hertzian Fracture,'' *J. Mater. Sci.*, **29**, 2216–30 (1994).

[72]R. Warren, ''Measurement of the Fracture Properties of Brittle Solids by Hertzian Indentation,'' *Acta Metall.*, **26**, 1759–69 (1978).

[73]K. L. Johnson, J. J. O'Connor, and A. C. Woodward, ''The Effect of Indenter Elasticity on the Hertzian Fracture of Brittle Materials,'' *Proc. R. Soc. London*, **A334**, 95 (1973).

[74]C. Kocer and R. E. Collins, ''The Angle of Hertzian Cone Cracks,'' *J. Am. Ceram. Soc.*, **81** [7] 1736–42 (1998).

[75]A. G. Evans and T. R. Wilshaw, ''Quasi-Plastic Solid Particle Damage in Brittle Materials,'' *Acta Metall.*, **24**, 939–56 (1976).

[76]F. Guiberteau, N. P. Padture, and B. R. Lawn, ''Effect of Grain Size on Hertzian Contact in Alumina,'' *J. Am. Ceram. Soc.*, **77** [7] 1825–31 (1994).

[77]N. P. Padture and B. R. Lawn, ''Toughness Properties of a Silicon Carbide with an *in Situ*-Induced Heterogeneous Grain Structure,'' *J. Am. Ceram. Soc.*, **77** [10] 2518–22 (1994).

[78]A. Pajares, L. Wei, B. R. Lawn, and D. B. Marshall, ''Damage Accumulation and Cyclic Fatigue in Mg-PSZ at Hertzian Contacts,'' *J. Mater. Res.*, **10** [10] 2613–25 (1995).

[79]H. H. K. Xu, L. Wei, N. P. Padture, B. R. Lawn, and R. L. Yeckley, ''Effect of Microstructural Coarsening on Hertzian Contact Damage in Silicon Nitride,'' *J. Mater. Sci.*, **30**, 869–78 (1995).

[80]R. M. Davies, ''Determination of Static and Dynamic Yield Stresses Using a Steel Ball,'' *Proc. R. Soc. London*, **A197** [1050] 416–32 (1949).

[81]S. K. Lee, S. Wuttiphan, and B. R. Lawn, ''Role of Microstructure in Hertzian Contact Damage in Silicon Nitride: I. Mechanical Characterization,'' *J. Am. Ceram. Soc.*, **80** [9] 2367–81 (1997).

[82]T. O. Mulhearn, ''The Deformation of Metals by Vickers-Type Pyramidal Indenters,'' *J. Mech. Phys. Solids*, **7**, 85–96 (1959).

[83]J. T. Hagan and M. V. Swain, ''The Origin of Median and Lateral Cracks at Plastic Indents in Brittle Materials,'' *J. Phys. D: Appl. Phys.*, **11** [15] 2091–102 (1978).

[84]L. An, H. M. Chan, N. P. Padture, and B. R. Lawn, ''Damage-Resistant Alumina-Based Layer Composites,'' *J. Mater. Res.*, **11** [1] 204–10 (1996).

[85]M. Belmonte and S. K. Lee, ''Contact Damage in Alumina Reinforced with Silicon Carbide Platelets,'' *J. Mater. Sci.*, **16**, 379–81 (1997).

[86]B. A. Latella, B. H. O'Connor, N. P. Padture, and B. R. Lawn, ''Hertzian Contact Damage in Porous Alumina Ceramics,'' *J. Am. Ceram. Soc.*, **80** [4] 1027–31 (1997).

[87]S. K. Lee, K. S. Lee, B. R. Lawn, and D. K. Kim, ''Effect of Starting Powder on Damage Resistance of Silicon Nitrides,'' *J. Am. Ceram. Soc.*, **81** [8] 2061–70 (1998).

[88]C. J. Fairbanks, B. R. Lawn, R. F. Cook, and Y.-W. Mai, ''Microstructure and the Strength of Ceramics''; pp. 23–37 in *Fracture Mechanics of Ceramics*, Vol. 8. Edited by R. C. Bradt, A. G. Evans, D. P. H. Hasselman, and F. F. Lange. Plenum, New York, 1986.

[89]L. An, K. Soni, and H. M. Chan, ''Control of Calcium Hexaluminate Grain Morphology in *In-Situ*-Toughened Ceramic Composites,'' *J. Mater. Sci.*, **31**, 3223–29 (1996).

[90]N. P. Padture, ''*In Situ* Toughened Silicon Carbide,'' *J. Am. Ceram. Soc.*, **77** [2] 519–23 (1994).

[91]A. Pajares, F. Guiberteau, B. R. Lawn, and S. Lathabai, ''Hertzian Contact Damage in Magnesia-Partially-Stabilized Zirconia,'' *J. Am. Ceram. Soc.*, **78** [4] 1083–86 (1995).

[92]D. T. Smith and L. Wei, ''Quantifying Local Microcrack Density in Ceramics: A Comparison of Instrumented Indentation and Thermal Wave Techniques,'' *J. Am. Ceram. Soc.*, **78** [5] 1301–304 (1995).

[93]L. Wei and G. S. White, ''Thermal Diffusivity Maps: Case Studies in Ceramics,'' *J. Mater. Res.*, **12** [9] 2381–87 (1997).

[94]L. Wei and B. R. Lawn, ''Thermal Wave Analysis of Contact Damage in Ceramics: Case Study on Alumina,'' *J. Mater. Res.*, **11** [4] 939–47 (1996).

[95]D. P. H. Hasselman, ''Effect of Cracks on Thermal Conductivity,'' *J. Compos. Mater.*, **12**, 403–407 (1978).

[96]H. Horii and S. Nemat-Nasser, ''Brittle Failure in Compression: Splitting, Faulting, and Brittle–Ductile Transition,'' *Philos. Trans. R. Soc. London*, **319** [1549] 337–74 (1986).

[97]J. M. Kemeny and N. G. W. Cook, ''Micromechanics of Deformation in Rock''; pp. 287–311 in *Toughening Mechanisms in Quasi-Brittle Materials.* Edited by S. P. Shah. Kluwer Academic Publishers, Dordrecht, The Netherlands, 1991.

[98]B. R. Lawn and D. B. Marshall, ''Nonlinear Stress–Strain Curves for Solids Containing Closed Cracks with Friction,'' *J. Mech. Phys. Solids*, **46** [1] 85–113 (1998).

[99]B. R. Lawn, S. K. Lee, I. M. Peterson, and S. Wuttiphan, ''A Model of Strength Degradation from Hertzian Contact Damage in Tough Ceramics,'' *J. Am. Ceram. Soc.*, **81** [6] 1509–20 (1998).

[100]A. V. Dyskin, R. J. Jewell, H. Joer, E. Sahouryeh, and K. B. Ustinov, ''Experiments on 3-D Crack Growth in Uniaxial Compression,'' *Int. J. Fract.*, **65** [4] R77–R83 (1994).

[101]S. K. Lee and B. R. Lawn, ''Role of Microstructure in Hertzian Contact Damage in Silicon Nitride: II. Strength Degradation,'' *J. Am. Ceram. Soc.*, **81** [4] 997–1003 (1998).

[102]A. G. Evans, ''Strength Degradation by Projectile Impacts,'' *J. Am. Ceram. Soc.*, **56** [8] 405–409 (1973).

[103]S. M. Wiederhorn and B. R. Lawn, ''Strength Degradation of Glass Resulting from Impact with Spheres,'' *J. Am. Ceram. Soc.*, **60** [9–10] 451–58 (1977).

[104]B. R. Lawn, D. B. Marshall, P. Chantikul, and G. R. Anstis, ''Indentation Fracture: Applications in the Assessment of Strength of Ceramics,'' *J. Aust. Ceram. Soc.*, **16** [1] 4–9 (1980).

[105]J. R. Kelly, ''Ceramics in Restorative and Prosthetic Dentistry,'' *Ann. Rev. Mater. Sci.*, **27**, 443–68 (1997).

[106]Y.-G. Jung, I. M. Peterson, A. Pajares, and B. R. Lawn, ''Contact Damage Resistance and Strength Degradation of Glass-Infiltrated Alumina and Spinel Ceramics,'' *J. Dent. Res.*, in press.

[107]I. M. Peterson, S. Wuttiphan, A. Pajares, and B. R. Lawn, ''Role of Microstructure on Contact Damage and Strength Degradation in Micaceous Glass-Ceramics,'' *Dent. Mater.*, in press.

[108]Y. G. Jung, S. Wuttiphan, I. M. Peterson, and B. R. Lawn, ''Damage Modes in Dental Layer Structures,'' *J. Dent. Res.*, in press.

[109]R. O. Ritchie, ''Mechanisms of Fatigue Crack Propagation in Metals, Ceramics, Composites: Role of Crack-Tip Shielding,'' *Mater. Sci. Eng.*, **A103**, 15–28 (1988).

[110]S. Suresh, *Fatigue of Materials.* Cambridge University Press, Cambridge, U.K., 1991.

[111]S. Lathabai, J. Rödel, and B. R. Lawn, ''Cyclic Fatigue from Frictional Degradation at Bridging Grains in Alumina,'' *J. Am. Ceram. Soc.*, **74** [6] 1340–48 (1991).

[112]H. Cai, M. A. S. Kalceff, B. M. Hooks, B. R. Lawn, and K. Chyung, ''Cyclic Fatigue of a Mica-Containing Glass-Ceramic at Hertzian Contacts,'' *J. Mater. Res.*, **9** [10] 2654–61 (1994).

[113]N. P. Padture and B. R. Lawn, ''Contact Fatigue of a Silicon Carbide with a Heterogeneous Grain Structure,'' *J. Am. Ceram. Soc.*, **78** [6] 1431–38 (1995).

[114]H. H. K. Xu and S. Jahanmir, ''Microfracture and Material Removal in Scratching of Alumina,'' *J. Mater. Sci.*, **30**, 2235–47 (1995).

[115]B. R. Lawn, N. P. Padture, F. Guiberteau, and H. Cai, ''A Model for Microcrack Initiation and Propagation Beneath Hertzian Contacts in Polycrystalline Ceramics,'' *Acta Metall.*, **42** [5] 1683–93 (1994).

[116]N. P. Padture and B. R. Lawn, ''Fatigue in Ceramics with Interconnecting Weak Interfaces: A Study Using Cyclic Hertzian Contacts,'' *Acta Metall.*, **43** [4] 1609–17 (1995).

[117]P. J. Kennedy, A. A. Conte, E. P. Whitenton, L. K. Ives, and M. B. Peterson, ''Surface Damage and Mechanics of Fretting Wear in Ceramics''; pp. 79–98 in *Friction and Wear of Ceramics.* Edited by S. Jahanmir. Marcel Dekker, New York, 1994.

[118]C. J. Russo, M. P. Harmer, H. M. Chan, and G. A. Miller, ''Design of a Laminated Ceramic Composite for Improved Strength and Toughness,'' *J. Am. Ceram. Soc.*, **75** [12] 3396–3400 (1992).

[119]H. M. Chan, ''Layered Ceramics: Processing and Mechanical Behavior,'' *Ann. Rev. Mater. Sci.*, **27**, 249–82 (1997).

[120]S. Wuttiphan, B. R. Lawn, and N. P. Padture, ''Crack Suppression in Strongly Bonded Homogeneous/Heterogeneous Laminates: A Study on Glass/Glass-Ceramic Bilayers,'' *J. Am. Ceram. Soc.*, **79** [3] 634–40 (1996).

[121]H. Liu, B. R. Lawn, and S. M. Hsu, ''Hertzian Contact Response of Tailored Silicon Nitride Multilayers,'' *J. Am. Ceram. Soc.*, **79** [4] 1009–14 (1996).

[122]K. S. Lee, S. Wuttiphan, X. Z. Hu, S. K. Lee, and B. R. Lawn, ''Contact-Induced Transverse Fractures in Brittle Layers on Soft Substrates: A Study on Silicon Nitride Bilayers,'' *J. Am. Ceram. Soc.*, **81** [3] 571–80 (1998).

[123]K. S. Lee, S. K. Lee, B. R. Lawn, and D. K. Kim, ''Contact Damage and Strength Degradation in Brittle/Quasi-Plastic Silicon Nitride Bilayers,'' *J. Am. Ceram. Soc.*, (in press).

[124]L. Wei, A. Pajares, and B. R. Lawn, ''Effect of Mechanical Damage on Thermal Conduction of Plasma Sprayed Coatings,'' *J. Mater. Res.*, **11** [6] 1329–32 (1996).

[125]A. Pajares, L. Wei, B. R. Lawn, N. P. Padture, and C. C. Berndt, ''Mechanical Characterization of Plasma-Sprayed Ceramic Coatings on Metal Substrates by Contact Testing,'' *Mater. Sci. Eng.*, **A208** [2] 158–65 (1996).

[126]A. C. Fischer-Cripps, B. R. Lawn, A. Pajares, and L. Wei, ''Stress Analysis of Elastic–Plastic Contact Damage in Ceramic Coatings on Metal Substrates,'' *J. Am. Ceram. Soc.*, **79** [10] 2619–25 (1996).

[127]A. Pajares, L. Wei, B. R. Lawn, and C. C. Berndt, ''Contact Damage in Plasma-Sprayed Alumina-Based Coatings,'' *J. Am. Ceram. Soc.*, **79** [7] 1907–14 (1996).

[128]S. Wuttiphan, A. Pajares, B. R. Lawn, and C. C. Berndt, ''Effect of Substrate and Bond Coat on Contact Damage in Zirconia-Based Plasma Coatings,'' *Thin Solid Films*, **293** [1–2] 251–60 (1997).

[129]H. Herman, ''Plasma-Sprayed Coatings,'' *Sci. Am.*, **256** [9] 113–88 (1988).

[130]M. V. Swain and J. Mencik, ''Mechanical Property Characterization of Thin Films Using Spherical Tipped Indenters,'' *Thin Solid Films*, **253**, 204–11 (1994).

[131]K. Komvopolous, ''Elastic–Plastic Finite Element Analysis of Indented Layered Media,'' *J. Tribology*, **111**, 430–39 (1989).

[132]P. Montmitonnet, M. L. Edinger, and E. Felder, ''Finite Element Analysis of Elastoplastic Indentation: Part II—Application to Hard Coatings,'' *J. Tribology*, **115**, 15–19 (1993).

[133]X. Z. Hu and B. R. Lawn, ''A Simple Indentation Stress–Strain Relation for Contacts with Spheres on Bilayer Structures,'' *Thin Solid Films*, in press.

[134]H. Liu and S. M. Hsu, ''Fracture Behavior of Multilayer Silicon Nitride/Boron Nitride Ceramics,'' *J. Am. Ceram. Soc.*, **79** [9] 2452–57 (1996).

[135]J. Jitcharoen, N. P. Padture, A. E. Giannakopoulos, and S. Suresh, ''Hertzian-Crack Suppression in Ceramics with Elastic-Modulus-Graded Surfaces,'' *J. Am. Ceram. Soc.*, in press. □

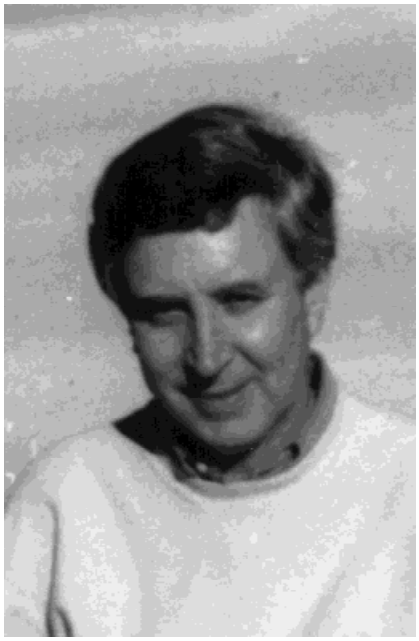

Brian R. Lawn gained his B.Sc. and Ph.D. degrees in physics at the University of Western Australia. After graduating, he was a Postdoctoral Fellow in the School of Physics at the University of Bristol and in the Department of Engineering and Materials Science at Brown University. Dr. Lawn then held a position as a lecturer in applied physics at the University of New South Wales for several years. During this tenure, he spent several periods of study leave in the Department of Materials Science at the University of Sussex and in the Ceramics Division at the National Institute of Standards and Technology (then the National Bureau of Standards). In 1981, Dr. Lawn joined the National Institute of Standards and Technology permanently, and, in 1987, was elected to the position of NIST Fellow. He currently holds appointments as Adjunct Professor in materials science at Lehigh University and the University of Maryland in the United States, and in applied physics at Curtin University in Western Australia. Dr. Lawn has published widely on the fracture properties of brittle materials, and is the author of *Fracture of Brittle Solids*, now in its second edition.

ERRATA

Errors in Hertzian stress field eqns. are corrected below:

Panel A: Hertzian Stress Fields

The stresses within the Hertzian elastic contact field are given by the following expressions, in cylindrical coordinates R,θ,z (with z along the axis of symmetry): [21,23]

$$\sigma_R/p_0 = {}^1/_2(1-2\nu)(a/R)^2\{1-(z/u^{1/2})^3\} + {}^3/_2(z/u^{1/2})^3\{a^2u/(u^2+a^2z^2)\} + {}^3/_2(z/u^{1/2})\{(1-\nu)u/(a^2+u) + (1+\nu)(u^{1/2}/a)\arctan(a/u^{1/2}) - 2\}$$

$$\sigma_\theta/p_0 = {}^1/_2(1-2\nu)(a/R)^2\{1-(z/u^{1/2})^3\} + {}^3/_2(z/u^{1/2})\{2\nu + (1-\nu)u/(a^2+u) - (1+\nu)(u^{1/2}/a)\arctan(a/u^{1/2})\}$$

$$\sigma_z/p_0 = -{}^3/_2(z/u^{1/2})^3\{a^2u/(u^2+a^2z^2)\}$$

$$\tau_{Rz} = -{}^3/_2\{Rz^2/(u^2+a^2z^2)\}\{a^2u^{1/2}/(a^2+u)\}$$

where

$$u = {}^1/_2\{(R^2+z^2-a^2) + [(R^2+z^2-a^2)^2 + 4\,a^2z^2]^{1/2}\}^{1/2}$$

The principal normal stresses, defined such that $\sigma_1 \geq \sigma_2 \geq \sigma_3$ nearly everywhere [11], are

$$\sigma_1 = {}^1/_2(\sigma_R+\sigma_z) + \{[{}^1/_2(\sigma_R+\sigma_z)]^2 + \tau_{rz}{}^2\}^{1/2}$$
$$\sigma_2 = \sigma_\theta$$
$$\sigma_3 = {}^1/_2(\sigma_R+\sigma_z) - \{[{}^1/_2(\sigma_R+\sigma_z)]^2 + \tau_{rz}{}^2\}^{1/2}$$

with σ_2 a hoop stress. The maximum principal shear stress is

$$\tau_{13} = {}^1/_2(\sigma_1-\sigma_3)$$

The angle α between the σ_2–σ_3 stress trajectory surface (closely approximating the cone crack path) and the specimen free surface is given by

$$\tan 2\alpha = -2\tau_{Rz}/(\sigma_R-\sigma_z)$$

Analogous relations exist for a cylindrical flat punch end-loaded onto the specimen surface [21] and for a sliding spherical indenter.[24,25]